Field:
Chemistry/Biochemistry

Session Topic:
Super-resolution Imaging

Chair:
Derek TOOMRE, Yale University

Essential knowledge of life comes from our ability to see cells and small structures within cells (e.g. organelles) and follow them over time. A common tool to see structures in live cells is fluorescent light microscopy, which has become even more popular with the advent of genetically encoded probes like green fluorescent protein (GFP); the latter had such a fundamental impact that in 2008 was the topic of the Nobel Prize of Chemistry. Despite the power of live cell imaging with conventional fluorescent microscopy, a major roadblock is what it can not do – resolve objects less than about have the wavelength of the illumination light. This barrier to distinguish objects is fundamentally limited by the properties of diffraction, long ago describe by Abbe (in 1873). While this barrier was taken as dogma of what can be seen by far-field microscopy, it has recently been shattered by a cadre of new nanoscopes that are collectively called 'super-resolution microscopy'.

These nanoscopes broke the diffraction barrier by carefully choosing contexts in which Abbe's law did not apply, such as through non-linear or near-field effect, selectively turning on and off dyes in a controlled or stochastic manner, and localizing single molecules (dyes) with tens of nanometer precisions. In this session, Dr. Derek Toomre will first present a brief overview of super-resolution imaging, emphasizing the advantages and limitations of different super-resolution approaches. Dr. Katsumasa Fujita will introduce the concept of super resolution microscopy using non-linear optical saturation effects to derive information beyond the diffraction limit. Dr. Bo Haung will then discuss a different super-resolution microscopy technique, Stochastic Optical Reconstruction Microscopy (STORM), which determines the position of each molecule of interest by switching molecules between a visible and an invisible state; images are built up point-by-point somewhat akin to a pointillism paintings of the impressionists. STORM allows one to resolve cellular features an order of magnitude smaller than conventional fluorescence microscopy and can be extended to three-dimensional and multicolor imaging. Both Drs Fujita and Haung demonstrate the potential of super-resolution imaging to provide more detailed understandings of biological processes at the cell level. With an eye towards the future, the potential, challenges and perhaps even new solutions will be active discussion points.

NanoString Exhibit 1018.001

ANNUAL REVIEWS **Further**

Click here for quick links to Annual Reviews content online, including:

- Other articles in this volume
- Top cited articles
- Top downloaded articles
- Our comprehensive search

Annu. Rev. Cell Dev. Biol. 2010.26:285-314. Downloaded from www.annualreviews.org
by Yale University STERLING CHEMISTRY LIBRARY on 10/08/10. For personal use only.

A New Wave of Cellular Imaging

Derek Toomre and Joerg Bewersdorf

Department of Cell Biology, Yale University School of Medicine, New Haven, Connecticut 06520-8002; email: derek.toomre@yale.edu, joerg.bewersdorf@yale.edu

Annu. Rev. Cell Dev. Biol. 2010. 26:285–314

The *Annual Review of Cell and Developmental Biology* is online at cellbio.annualreviews.org

This article's doi:
10.1146/annurev-cellbio-100109-104048

Copyright © 2010 by Annual Reviews.
All rights reserved

1081-0706/10/1110-0285$20.00

Key Words

super-resolution, light microscopy, total internal reflection fluorescence microscopy (TIRFM), live cell imaging, fluorescence, single molecule

Abstract

Fluorescence imaging methods that push or break the diffraction limit of resolution (approximately 200 nm) have grown explosively. These super-resolution nanoscopy techniques include: stimulated emission depletion (STED), Pointillism microscopy [(fluorescence) photoactivation localization microscopy/stochastic optical reconstruction microscopy, or (F)PALM/STORM], structured illumination, total internal reflection fluorescence microscopy (TIRFM), and those that combine multiple modalities. Each affords unique strengths in lateral and axial resolution, speed, sensitivity, and fluorophore compatibility. We examine the optical principles and design of these new instruments and their ability to see more detail with greater sensitivity—down to single molecules with tens of nanometers resolution. Nanoscopes have revealed transient intermediate states of organelles and molecules in living cells and have led to new discoveries but also biological controversies. We highlight common unifying principles behind nanoscopy such as the conversion of a subset of probes between states (ground or excited) and the use of scanning (ordered or stochastic). We emphasize major advances, biological applications, and promising new developments.

NanoString Exhibit 1018.002

Annu. Rev. Cell Dev. Biol. 2010.26:285-314. Downloaded from www.annualreviews.org
by Yale University STERLING CHEMISTRY LIBRARY on 10/08/10. For personal use only.

Contents

FOREWORD: SEEING THE NANOSCOPIC WORLD 286
THE LIGHT BARRIER: RESOLUTION IS LIMITED 287
A Primer 287
Pushing the Resolution Limit 287
Exploiting Probes and Shattering Barriers 289
SUPER-RESOLUTION MICROSCOPY 290
Structured Illumination Microscopy 290
Stimulated Emission Depletion Microscopy 290
Pointillism Microscopy 293
Cellular Applications with Super-Resolution 297
No Single Winner: Super-Resolution Trade-Offs 300
AXIAL SUPER-RESOLUTION WITH TOTAL INTERNAL REFLECTION FLUORESCENCE MICROSCOPY 300
A Primer 300
Total Internal Reflection Fluorescence Microscopy Instrumentation 302
Cellular Applications with Total Internal Reflection Fluorescence Microscopy 303
LOOKING BACK AND PROJECTING FORWARD 306

FOREWORD: SEEING THE NANOSCOPIC WORLD

In the 1960s, a *nouvelle vague* (new wave) of cinematographers broke rank with classic paradigms, and with fresh perspectives and new techniques, breathed new life into French cinema. More recently, James Cameron used innovative stereo videocameras and computer animation to immerse audiences in *Avatar*'s quasi-real 3D world.

Far-field: regime distant from the objective lens (utilized in most microscopes)

Imaging of the cellular world is experiencing an even more radical renaissance. In roughly a decade, an international cadre of pioneering scientists have challenged (or more accurately, circumnavigated) what was taken as dogma to be the hard limit of what could be visualized by far-field light microscopy: Abbe's limit of resolution (~200 nm laterally). The diffraction light barrier was broken by carefully choosing contexts in which Abbe's law did not apply, such as through exploiting nonlinear or near-field effects, selectively turning dyes on and off, and localizing single fluorophores with high precision. Armed with new photoswitchable probes and video nanoscopes, a surge of super-resolution techniques has allowed scientists to peer inside living cells with an unprecedented level of resolution and sensitivity. Imagine seeing single molecules at work inside living cells or using light to control their interactions in space and time. Such quests are no longer fanciful visions but instead just within our reach, albeit with many challenges. By pushing the laws of optics and materials, the photochemical states of dyes, and genetic molecular engineering, the race is on to see within living cells with more detail, sensitivity, and speed—and to apply these tools to interrogate how cells function.

In this review, we emphasize new developments and applications of super-resolution optical methods. As stimulated emission depletion (STED) microscopy, (fluorescence) photoactivation localization microscopy/stochastic optical reconstruction microscopy [(F)PALM/STORM], structured illumination microscopy (SIM), and total internal reflection fluorescence microscopy (TIRFM) instruments are now commercially available, biologists who wish to use them will need to make informed choices, as with each there are trade-offs between sensitivity, resolution, field and depth of view, speed, and probe versatility. This review is divided into two parts. First, after describing the limitations of traditional microscopy, we explore how new nanoscopes

NanoString Exhibit 1018.003

work and then give early examples that show their benefit to cell biology and potential. Second, we discuss TIRFM, a long-established axial super-resolution technique, with emphasis on new advances and its larger gamut of applications.

As much as possible, we have tried to take a biologist's perspective by focusing on key principles and directly comparing the instruments' advantages and limitations with examples of their use in addressing cellular problems. With emphasis on the nanoscale, we bypass exciting advances in millimeter-scale imaging such as selective plane illumination microscopy (SPIM) (Keller et al. 2008) and multiphoton imaging (Dunn & Sutton 2008). We also encourage the interested reader to refer to in-depth reviews on biological probes (Fernandez-Suarez & Ting 2008), TIRFM (Axelrod 2008), and super-resolution microscopy (Hell 2007, Huang et al. 2009, Patterson et al. 2010).

THE LIGHT BARRIER: RESOLUTION IS LIMITED

A Primer

In light microscopy, resolution is fundamentally limited by the properties of diffraction (Abbe 1873). Diffraction causes sharp point-like objects, such as the dots in **Figure 1*a*,*b***, to appear blurry. The details that can be seen—or not seen—by a microscope are determined by its resolution.

Resolution can be quantified by analyzing a microscope's point-spread function (PSF), which effectively describes how blurry a point-like object (a single molecule or small fluorescent bead) (**Figure 1*b***) will appear. A cross section of the lateral PSF generates a pattern that is often in the shape of an Airy disk (**Figure 1*c***) (Pawley 2005). The PSF's full-width at half-maximum (FWHM) value (**Figure 1*c***) is a simple way to characterize the resolution in the x, y, and z directions. The Raleigh criterion states that two points are resolvable if their distance d is at least the radius r_{Airy} of an Airy disk-shaped PSF (**Figure 1*c***), described by the formula

$$d \geq r_{\mathrm{Airy}} \approx 0.61\ \lambda_0/NA \approx \mathrm{PSF}_{\mathrm{FWHM}}, \quad 1.$$

whereby λ_0 represents the wavelength and NA the numerical aperture of the objective. Thus, resolution is improved at short wavelengths and high NA. The axial resolution can be approximated by the formula $d_z \approx n\lambda_0/NA^2$, with n being the refractive index, and is typically 2 to 3 times worse than the lateral resolution. λ_0 and NA are both at their limit: the first by the incompatibility of short wavelength UV light with biological specimens, the second by modern high-NA objectives (e.g., 1.49 NA) with half aperture angles already approaching the theoretical limit of 90°. The PSF dimensions of conventional microscopes are therefore limited to FWHMs of 200–250 nm in the x and y directions, and 500–700 nm in the z axis.

Confocal laser scanning microscopy (CLSM) is equally bound by these limits: The scanning spot for illumination is still diffraction-limited, as is imaging through the pinhole or slit. The latter rejects out-of-focus background light and improves the contrast (Pawley 2005); however, in practice it does not significantly improve resolution beyond a conventional wide-field microscope, except at extremely small pinhole diameters (**Figure 1*e***).

In contrast, TIRFM or scanning near-field optical microscopy (SNOM) use near-field excitation, which is not bound by diffraction laws and allows sub-100 nm resolution. However, near-field microscopy is generally limited to observations close to the cell surface. Starting approximately two decades ago, far-field methods that can interrogate the entire cell were developed that pushed and eventually shattered Abbe's resolution limit.

Pushing the Resolution Limit

Multiple strategies have pushed the envelope of what can be resolved by light microscopy by exploiting, in innovative ways, the maximal possible NA.

Resolution: the minimum distance at which objects can be distinguished when imaged with a microscope; often characterized by the full width half maximum of the point-spread function

Diffraction: bending of light at obstacles (e.g., apertures), which restricts how well light can be focused and limits the resolution of microscopes

Near-field: regime dominated by evanescent waves (the light contributions that vanish within one wavelength) and utilized in total internal reflection fluorescence microscopes

Super-resolution: techniques that can resolve objects (or details) smaller than the classical diffraction barrier

Stimulated emission: photophysical process by which, through stimulation by light, an excited fluorophore relaxes to its ground state and thus prevents fluorescence emission

STED: stimulated emission depletion

(F)PALM: (fluorescence) photoactivation localization microscopy

STORM: stochastic optical reconstruction microscopy

Annu. Rev. Cell Dev. Biol. 2010.26:285-314. Downloaded from www.annualreviews.org
by Yale University STERLING CHEMISTRY LIBRARY on 10/08/10. For personal use only.

NanoString Exhibit 1018.004

Annu. Rev. Cell Dev. Biol. 2010.26:285-314. Downloaded from www.annualreviews.org
by Yale University STERLING CHEMISTRY LIBRARY on 10/08/10. For personal use only.

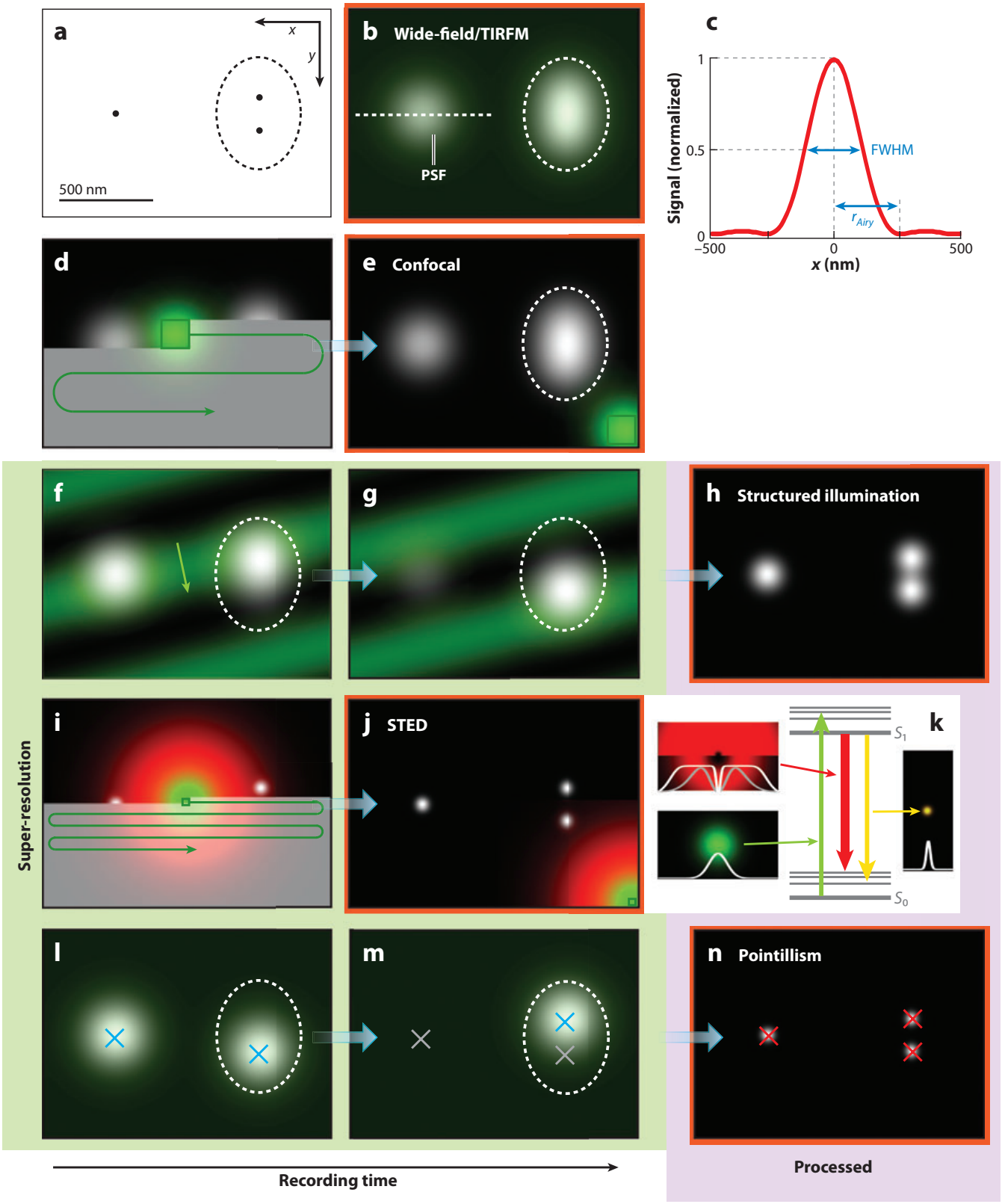

NanoString Exhibit 1018.005

Annu. Rev. Cell Dev. Biol. 2010.26:285-314. Downloaded from www.annualreviews.org
by Yale University STERLING CHEMISTRY LIBRARY on 10/08/10. For personal use only.

Gaining an edge by deconvolution. As shown in Equation 1, *NA* governs resolution. The outermost angles in high-NA objectives are responsible for the resolution advantage over low-NA lenses. Deconvolution microscopy (McNally et al. 1999) amplifies spatial signals in a recorded image that the high transmission angles contributed. This computationally intensive postprocessing technique greatly decreases background noise and can enhance resolution.

Two are better than one: combining two objective lenses. In 4Pi microscopy, the sample is illuminated by one light source from two opposing objectives, which generates a focused standing wave. Emitted light is collected by both objectives, merged, and detected. Optically, the two objective lenses act as one unit with an effectively doubled NA. Even better, the light is now incident (and detected) from a much larger range of directions, including opposing paths. This results in a dramatic axial sharpening of the PSF as its $FWHM_{\text{axial}} \approx 100$ nm (Gugel et al. 2004, Hell & Stelzer 1992). Whereas 4Pi microscopy is based on a confocal geometry, I^5M (Gustafsson et al. 1999), which has a similar dual-lens arrangement, achieves equivalent resolution (Bewersdorf et al. 2006) using a lamp and a camera in a wide-field configuration.

Exploiting numerical aperture in illumination. The resolution performance of regular wide-field fluorescence microscopy depends solely on the detection path. SIM takes maximum advantage of the objective's NA for illumination. Placing, for example, a spatial mask in the light path creates a fine pattern of illumination stripes in the sample. This pattern is scanned or rotated, which allows different parts of adjacent structures to be illuminated at different times (see **Figure 1*f*,*g***). Computational postprocessing of these oscillating patterns renders images at approximately double the resolution of conventional microscopy (**Figure 1*b***) (Gustafsson et al. 2008).

Exploiting Probes and Shattering Barriers

The methods above maximize resolution by enhancing the optical performance of the instrument. In contrast, two other super-resolution strategies rely on photophysical properties of fluorescent probes to enhance resolution. This focus on the probes was a critical frameshift in breaking the diffraction barrier (Hell & Wichmann 1994). Specifically, the switching on and off of fluorophores in a binary fashion was exploited. These two general approaches are:

1. STED microscopy (Hell & Wichmann 1994), which relies on targeted PSF

SIM: structured illumination microscopy

TIRFM: total internal reflection fluorescence microscopy (also called evanescent wave microscopy)

Point-spread function (PSF): spatial distribution of light emitted by an infinitesimal source when observed in a microscope

FWHM: full-width at half-maximum

Numerical aperture (NA): $NA = n \sin \alpha$, whereby n is the refractive index and α the objective's half aperture angle

CLSM: confocal laser scanning microscopy

Figure 1

Comparison of selected modern microscopy techniques. (*a*) Hypothetical sample featuring three fluorescent molecules, here denoted by black points, located in the focal *x-y* plane. Two of them, indicated by the dashed oval, are closer than the Rayleigh resolution limit. They are therefore not resolvable in a wide-field microscope or total internal reflection fluorescence microscope (TIRFM) (*b*). Imaging the single particle permits determination of the point-spread function (PSF) of the microscope. Its intensity profile, measured along the straight dashed line in (*b*), is shown in (*c*). The PSF can be characterized by the full-width at half-maximum (FWHM) or the radius of the Airy disk, r_{Airy}, as shown in (*c*). (*d*,*e*) Confocal microscopy achieves a comparable *x-y* resolution by scanning the sample with a laser focus. (*f*–*h*) Structured illumination microscopy (SIM) relies on scanning the sample with a stripe pattern of excitation light that highlights the objects at different times (*f*,*g*). Postprocessing of the recorded images at different stripe positions yields the super-resolved image (*h*). (*i*–*k*) Stimulated emission depletion (STED) microscopy scans the sample with a laser spot for excitation (*green spot*) accompanied by a second doughnut-shaped laser focus (*red ring*). As shown in (*k*), this second light can stimulate emission of light (*red arrow* in the term scheme, representing the fluorophore) before spontaneous fluorescence relaxation can occur (*yellow arrow*). Increasing the stimulation light intensity drives the depletion process into saturation, as depicted by the upper half of the red ring, causing efficient fluorescence quenching even closer to the ring center and dramatically reducing the remaining fluorescence spot size (*yellow spot*). (*l*–*n*) Pointillism microscopy utilizes the random activation of single fluorophores. Sparsely distributed fluorescent molecules can be localized precisely in each recorded image (*crosses* in *l*,*m*). After recording many frames, the final image can be constructed from all determined positions (*n*). Red boxes illustrate the final *xy* images of the different microscopy methods.

NanoString Exhibit 1018.006

Pointillism microscopy: methods that combine large numbers of localized centers of single molecule images into a super-resolved image

Annu. Rev. Cell Dev. Biol. 2010.26:285-314. Downloaded from www.annualreviews.org
by Yale University STERLING CHEMISTRY LIBRARY on 10/08/10. For personal use only.

engineering to effectively reshape the illumination spot (Hell & Wichmann 1994), and

2. the Pointillism microscopy methods of (F)PALM, STORM, and other variants. This generates an image using random switching events; the final image is constructed from localized spots of single fluorophores and is remarkably similar to the Pointillism artwork of the neo-impressionists.

SUPER-RESOLUTION MICROSCOPY

Many resolution-enhancing techniques have been developed. We will concentrate on optical methods that have high potential for cellular imaging and are commercially available. These nanoscopy techniques are: SIM, STED microscopy, Pointillism microscopy, and TIRFM.

Structured Illumination Microscopy

When a fine pattern of stripes is projected onto a sample, their features are blurred when detected. However, if the stripes are moved across the specimen, a characteristic signal variation in the fluorescence response can be observed as a function of time and position. This is especially noticeable when examining sparsely distributed structures such as the adjacent dots in **Figure 1*f*,*g***.

SIM records a series of images with stripes at different, well-defined positions. By analyzing the signal variations between images, smaller structural features can be resolved than would be visible by regular microscopy (Gustafsson 2000). Because structures oriented parallel to the stripes do not benefit from this effect, the stripes are not only shifted but also rotated between images. Typically, SIM records frames at three different stripe orientations with three to five shift positions, resulting in 9–15 frames per final super-resolution SIM image (Gustafsson 2008). SIM is a hybrid technique: It images the whole field of view at once in the manner of a standard wide-field microscope, but it also relies on scanning the specimen with the stripe pattern, akin to confocal microscopy with the illumination spot.

Scanning is required to improve lateral resolution. Any far-field microscope that significantly enhances lateral resolution requires scanning, or more generally, sequential collection of data. The optical detection path is always diffraction limited and hence subject to identical constraints as regular microscopy. The controlled spatial confinement of the fluorescence-emitting area is essential for super-resolution to separate structures closer than the diffraction limit. This, however, implies that the whole sample is not excited at once, which in turn requires multiple excitation patterns to cover the whole field of view. Thus, spatial resolution is gained at the loss of temporal resolution.

Data processing. Sequential data collection requires the final image to be put together from single raw frames after data recording. In SIM, this means automatically analyzing for each pixel the signal variations between the different images. Typically, a Fourier transform–based algorithm is used that distinguishes sharp image components from signal oscillations to generate a super-resolution image (Gustafsson 2000). Two- or three-dimensional data sets can be obtained this way, typically at approximately twice the resolution in all dimensions, i.e., ~100–125 nm laterally and ~250 nm axially (Gustafsson et al. 2008). A major advantage of SIM is that it is compatible with most fluorophores and samples prepared for confocal (or wide-field deconvolution) microscopy. However, the enhanced resolution comes with a trade-off in speed (see **Table 1**).

Stimulated Emission Depletion Microscopy

The illumination spot in a CLSM samples the specimen; its size determines the resolution of the microscope because the spot blurs all structures. No matter how hard

NanoString Exhibit 1018.007

Table 1 Comparison of microscopy methods[a]

		Wide-field and confocal	TIRF	Structured illumination	STED	Pointillism
***x-y*-resolution**	Typ. Best	200–250 nm ○	200–250 nm ○	130 nm 100 nm ●	25–80 nm <10 nm ●●	25–40 nm ~10 nm ●●
***z*-resolution**	Typ. Best	500–700 nm ○	100 nm 30–80 nm ●●	250 nm 200 nm ●	150–600 nm 30 nm ●●	60 nm–none ~10 nm ●●
Depth (max)	Typ. Best	5–20 μm >50 μm (2PE[b]) ●●	~200 nm (500 nm)[c] ○/●●	5 μm 20 μm ●	5 μm 20 μm ●	100 nm–1 μm 10 μm ○
Speed, large field of view	Typ. Best	1–10 im. s^{-1} 30–100 im. s^{-1} ●●	1–10 im. s^{-1} 30–100 im. s^{-1} ●●	0.1–1 im. s^{-1} ~10 im. s^{-1} ●	0.05–0.3 im. s^{-1} ~1 im. s^{-1} ●	0.001 im. s^{-1} ~0.1 im. s^{-1} ○
Speed, small field of view	Typ. Best	Similar to above ●●	Similar to above ●●	Similar to above ●	~1 im. s^{-1} 10–60 im. s^{-1} ●●	Similar to above ○
Fluorophore flexibility		High ●●	High ●●	High ●●	STED compatible ●	Preferably photoswitchable ●
Sensitivity		Moderate ●	Very high ●●	Moderate ●	Moderate ●	High ●●
Bleaching		Moderate ●	Very low ●●	Moderate to high ●/○	High ○	High ○
Live cell		●●	●●	●	●	○
Multicolor (number of channels)	Typ. Best	1–2 3–5 ●●	1–2 3–4 ●●	1 2–4 ●	1 2 ○	1 2–8 ●
Instrument complexity		Low/medium[d] ●/●●	Medium ●	Medium ●	High ○	Low–high ●● – ○
Data processing		Not required ●●	Not required ●●	Required ○	Not required ●●	Required ○
Pros		Established Fast High flexibility	Compatible with wide-field Established Fast Background suppression	Compatible with wide-field	High resolution Fast for small fields of view No data processing	High resolution Relatively simple setup
Cons		Low resolution	No deep imaging	Limited resolution improvement Data processing	Fluorophore-limited Multicolor-limited	Fluorophore-limited Data processing

[a]○ – poor; ● – good; ●● – excellent.
[b]Multiphoton microscopy.
[c]The low depth penetration can be positive or negative, depending on the application.
[d]Wide-field, low; confocal, medium.
Abbreviations: NA, numerical aperture; Typ, typical; im., images.

Annu. Rev. Cell Dev. Biol. 2010.26:285-314. Downloaded from www.annualreviews.org
by Yale University STERLING CHEMISTRY LIBRARY on 10/08/10. For personal use only.

NanoString Exhibit 1018.008

one tries, a light beam cannot be focused more tightly than the diffraction limit. To achieve super-resolution microscopy, STED exploits photophysical characteristics of the probe molecules in combination with suitable lasers and optics (Hell & Wichmann 1994).

Photophysics. As in CLSM, probe molecules are excited by a focused laser beam (see the Jablonski diagram in **Figure 1*k***; e.g., 640 nm). Before spontaneous emission of fluorescence occurs (e.g., after a few nanoseconds) a second red-shifted (e.g., 740 nm), doughnut-shaped laser beam illuminates the sample (**Figure 1*i–k***). This second "STED beam" forces molecules, except for those in the doughnut hole, from their excited electronic state back to their ground state by stimulating emission of a photon of the same wavelength. A bandpass filter (e.g., 650–730 nm) rejects the stimulated photons (740 nm), whereas shorter wavelength fluorescence photons (from the hole) are collected. Thus, STED can effectively switch off a subset of fluorophores. The PSF-engineered STED doughnut that is centered on the excitation focus is responsible for the enhanced resolution (Klar et al. 2000). Fluorescence quenching occurs mainly at the periphery, whereas the intensity-free hole of the doughnut has no effect on the fluorescence emission.

Resolution depends on laser power. Increasing the intensity of the doughnut-shaped STED beam dramatically improves the resolution: even at the inner slope of the beam's ring profile, fluorophores are now switched off, which further sharpens the remaining fluorescent spot to a size much smaller than the diffraction-limited focus (compare yellow and green spots in **Figure 1*k***). Scanning the sample with this sharpened effective focus provides super-resolution images (**Figure 1*i,j***). The *x-y* resolution depends on the diffraction-limited resolution and is a function of its FWHM and the STED beam intensity measured relative to a saturation value:

$$FWHM_{STED} \approx FWHM/\sqrt{I/I_S + 1}. \qquad 2.$$

In this equation, *FWHM* is the width of the diffraction-limited focus, I stands for the maximum STED laser intensity in the sample, and I_S denotes the characteristic saturation intensity, a probe property that describes the STED beam intensity at which the remaining fluorescence is reduced to half its original level (Harke et al. 2008a). Typically 30–80 nm *x*-*y* resolution is achieved (Meyer et al. 2008, Moneron et al. 2010, Schröder et al. 2009), and recently less than even 10 nm FWHM was obtained (Rittweger et al. 2009). Practically, this requires lasers with several hundred milliwatts of power, approximately 1000 times the typical laser intensity in a confocal focus, but at a red-shifted wavelength such that typically no strong absorption is observed.

Three-dimensional and multicolor imaging. Improved lateral resolution can also be combined with enhanced axial resolution. With an alternatively shaped STED beam, additional axially-shifted intensity lobes can be created that quench the axial extension of the PSF (Harke et al. 2008b, Klar et al. 2000). A more efficient approach combines STED microscopy with a 4Pi-type dual objective geometry (Dyba & Hell 2002). Based on this method, Schmidt et al. recently demonstrated 30–45 nm resolution in 3D with their isoSTED system (Schmidt et al. 2008, 2009) (see **Figure 2*a–e***). Multicolor imaging in STED microscopy is challenging because two laser wavelengths are required for each dye; nonetheless, it is possible (Meyer et al. 2008). Combining a conventional fluorophore with a second fluorophore with a similar emission spectrum but a large Stokes shift between excitation and emission, can allow the use of a single STED laser for both dyes and simplifies the technique (Schmidt et al. 2008). While the dye choice is currently somewhat limiting, a large advantage of STED imaging is that it is relatively fast for small fields of view and requires no data postprocessing (**Table 1**).

Instead of STED: other point-spread function engineering methods. The photophysical principle of PSF engineering–based

Annu. Rev. Cell Dev. Biol. 2010.26:285-314. Downloaded from www.annualreviews.org
by Yale University STERLING CHEMISTRY LIBRARY on 10/08/10. For personal use only.

NanoString Exhibit 1018.009

super-resolution is not limited to stimulated emission. The important photophysical property is the saturation intensity (see Equation 2). Generally, any photophysical switching process classified under the term RESOLFT (reversible saturable optical fluorescence transitions) is suitable for nanoscopy (Hell 2003). Indeed, apart from stimulated emission RESOLFT imaging has been demonstrated by several approaches including ground state depletion (Bretschneider et al. 2007, Hell & Kroug 1995), quantum dot switching (Irvine et al. 2008), and switching between conformational states in photoswitchable fluorescent proteins (FPs) (Hofmann et al. 2005, Schwentker et al. 2007) or organic dyes (Bossi et al. 2006). In a SIM-based approach, saturation of fluorophore excitation can create sharper stripe minima and higher resolution images (Gustafsson 2005, Heintzmann et al. 2002).

Pointillism Microscopy

With most microscopy approaches, fluorescent probes are too densely distributed to be individually resolvable. Pointillism microscopy [a term coined in Lidke et al. (2005)] exploits the ability to clearly visualize single fluorophores to create a super-resolution image.

Localizing instead of resolving. The center of a PSF can be determined with much higher precision than its FWHM, as has been utilized with great success in particle-tracking microscopy for decades (Gelles et al. 1988, Yildiz et al. 2003). Pointillism microscopy exploits this phenomenon by sequentially switching single fluorescence molecules on and off and imaging them with a camera (**Figure 1*l*,*m***). The image of every molecule is then analyzed computationally to determine its subpixel position. The localization precision in each direction can be approximated by

$$FWHM_{\mathrm{loc}} \approx FWHM/\sqrt{N}, \qquad 3.$$

where *FWHM* is given by the PSF's dimension and *N* is the number of detected photons from a single molecule (assuming negligible background signal), which ranges from ~100–500 photons for FPs to ~6000 for cyanine dyes (Fernandez-Suarez & Ting 2008).

Switching enables localization of thousands of molecules. The Pointillism microscopy breakthrough occurred in 2006 with three independent publications that combined localization techniques with photoswitchable markers. These techniques have been termed PALM (Betzig et al. 2006), FPALM (Hess et al. 2006), and STORM (Rust et al. 2006). The use of photoswitchable markers (including photoactivatable markers) is a powerful approach to control the density of fluorescent molecules and has enabled cellular imaging of organelles that contain large numbers of markers.

The on-switching or activation light (often ~405 nm) switches a subset of dark dyes into an excitable conformation. These activated molecules can, in turn, be excited by a second light source (typically 488–561 nm) to emit fluorescence. Off-switching usually occurs by spontaneous "bleaching" after many fluorescence excitation cycles. Both activation and excitation light beams illuminate the sample homogeneously; their intensities are balanced so that well-separated spots can be recorded in each camera frame.

In contrast to STED microscopy, in which molecules are switched in a targeted fashion defined by the doughnut's shape, Pointillism microscopy randomly activates molecules. Instead of scanning the sample pixel by pixel, 100–100,000 camera frames are recorded from which sparsely distributed single molecule images are extracted and the molecules localized by computationally finding their centers. The bleaching of activated fluorophores and continuous activation of new ones (Egner et al. 2007) eventually leads to imaging of a large fraction of the fluorophore population. Summing all the localized spots (see **Figure 1*n*** for a simple example) results in a super-resolution image with an *x*-*y* resolution $FWHM_{\mathrm{loc}}$ of typically 20–30 nm, albeit at typical acquisition rates of several minutes.

RESOLFT: reversible saturable optical fluorescence transitions

Localization precision: uncertainty in determining a position

Annu. Rev. Cell Dev. Biol. 2010.26:285-314. Downloaded from www.annualreviews.org
by Yale University STERLING CHEMISTRY LIBRARY on 10/08/10. For personal use only.

NanoString Exhibit 1018.010

Variations in the switching mechanism. Pointillism microscopy can be realized in many ways. **Table 2** gives an overview of some of the currently preferred fluorescent markers. Early versions of Pointillism microscopy utilized the spontaneous blinking of quantum dots (Lidke et al. 2005) or the stepwise bleaching of conventional dyes (Gordon et al. 2004, Qu et al. 2004) to resolve ensembles of a few probes only tens of nanometers apart, but these versions lacked separate activation mechanisms.

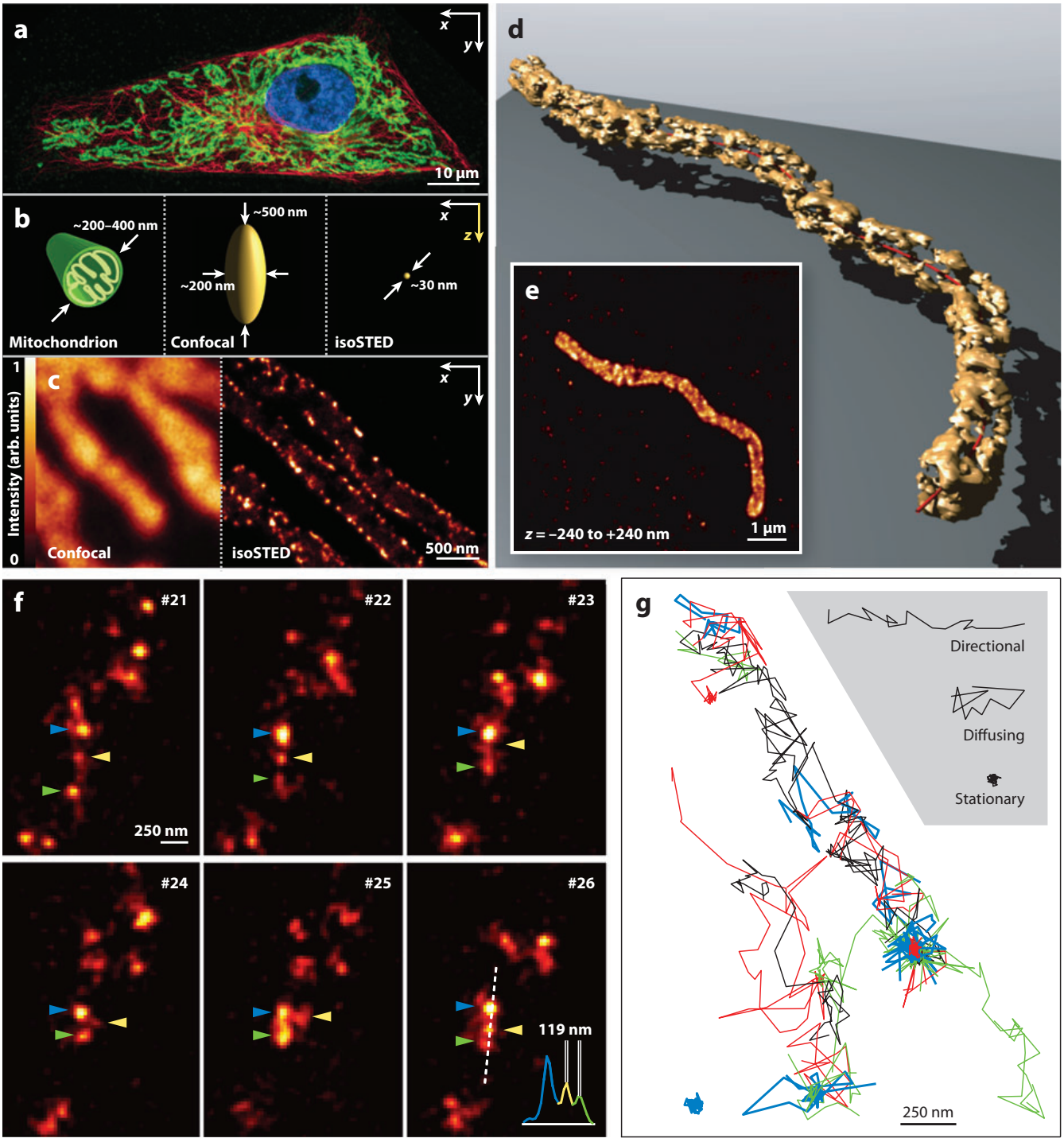

Annu. Rev. Cell Dev. Biol. 2010.26:285-314. Downloaded from www.annualreviews.org
by Yale University STERLING CHEMISTRY LIBRARY on 10/08/10. For personal use only.

NanoString Exhibit 1018.011

Table 2 A selection of preferred markers for Pointillism microscopy

Probe type	Probe	Comment	Selected references
Specialized fluorescent proteins			
Photo-activatable FP	PA-GFP, PA-mCherry	FPs that switch irreversibly from a nonfluorescent to a fluorescent state upon irradiation with 405 nm light	Patterson & Lippincott-Schwartz (2002), Subach et al. (2009)
Photo-shiftable FP	PS-CFP2, Dendra2, mEos2	Similar to PA FPs but switch from one fluorescence color to another	Chudakov et al. (2004), Gurskaya et al. (2006), McKinney et al. (2009)
Specialized organic probes			
Cyanine dye pairs	Cy3-Cy5 pair	Fluorescence of Cy5 is imaged. Cy5 can be rescued after bleaching by irradiation at the Cy3 wavelength. Alternative dye pairs: Donor: Alexa 405, Cy2, Cy3 Reporter: Cy5, Alexa 647, Cy5.5, Cy7	Bates et al. (2007) Conley et al. (2008)
Photo-switchable organic dyes	PS rhodamines, PA DCDHF cyanine dyes (Alexa 647)	Dyes can be reversibly or irreversibly switched on by light of a lower wavelength than the fluorescence excitation wavelength	Bossi et al. (2008) Pavani et al. (2009a) van de Linde et al. (2008)
Conventional fluorescent probes			
Regular organic dyes and FPs	Alexa dyes, atto dyes, and other FPs (GFPs, YFPs)	High intensities of fluorescence excitation light drive molecules into dark states from which they spontaneously recover	Baddeley et al. (2009), Fölling et al. (2008), Heilemann et al. (2008)
Weakly binding probes	Nile red and other dyes	These probes utilize the on- and off-rates of binding kinetics instead of photophysical activation and/or bleaching	Sharonov & Hochstrasser (2006)

FP, fluorescent protein; PA, photoactivatable; GFP, green fluorescent protein; PS, photoswitchable; CFP, cyan fluorescent protein; DCDHF, dicyanomethylenedihydrofuran; YFP, yellow fluorescent protein.

Although two light sources are a convenient way to control the frequency of activated versus bleached molecules in each frame, Pointillism microscopy can also resolve biological structures with just one light source and conventional dyes by driving them into dark states through high-intensity irradiation (Fölling et al. 2008, Heilemann et al. 2008)

Figure 2

Examples of STED microscopy. (*a*) Overview of the mitochondrial network in a PtK2 cell, including the transporter outer membrane (TOM) complex located on the outer mitochondrial membrane (*green*), β-tubulin (*red*), and DAPI (*blue*). (*b*) Size comparison of a mitochondrial tubule, a conventional confocal resolution volume, and a resolution volume of the 3D isoSTED microscope featuring a 3D resolution of approximately 30 nm. (*c*) TOM-complex-labeled mitochondria imaged in confocal (*left*) and isoSTED mode (*right*). (*d*) Three-dimensional reconstruction of an isoSTED data set of a similar structure (Tom20 immunolabeling). (*e*) Sum of all *x*-*y* images over a 480-nm range, which mimics 2D STED with conventional confocal *z*-resolution and shows that 3D super-resolution is essential for unraveling the protein distribution on the suborganelle level. (*f*) Selection of six time points from a STED movie of immunolabeled synaptic vesicles in a cultured neuron recorded at 28 frames s^{-1}. The colored arrowheads indicate three tracked vesicles. The profile in the last image demonstrates that two of the vesicles can be resolved along the dashed line even though they are only 119 nm apart. (*g*) Vesicle traces, some of which show vesicles seemingly getting trapped, whereas others are reminiscent of active transport. Trace examples are shown in the inset. (*a–c*) Adapted with permission from Schmidt et al. (2009), copyright © 2009 American Chemical Society. (*d*,*e*) Adapted with permission from Macmillan Publishers Ltd., *Nature Methods*, Schmidt et al. (2008), copyright © 2008. (*f*,*g*) From Westphal et al. (2008); reprinted with permission from AAAS.

Annu. Rev. Cell Dev. Biol. 2010.26:285-314. Downloaded from www.annualreviews.org
by Yale University STERLING CHEMISTRY LIBRARY on 10/08/10. For personal use only.

NanoString Exhibit 1018.012

Annu. Rev. Cell Dev. Biol. 2010.26:285-314. Downloaded from www.annualreviews.org
by Yale University STERLING CHEMISTRY LIBRARY on 10/08/10. For personal use only.

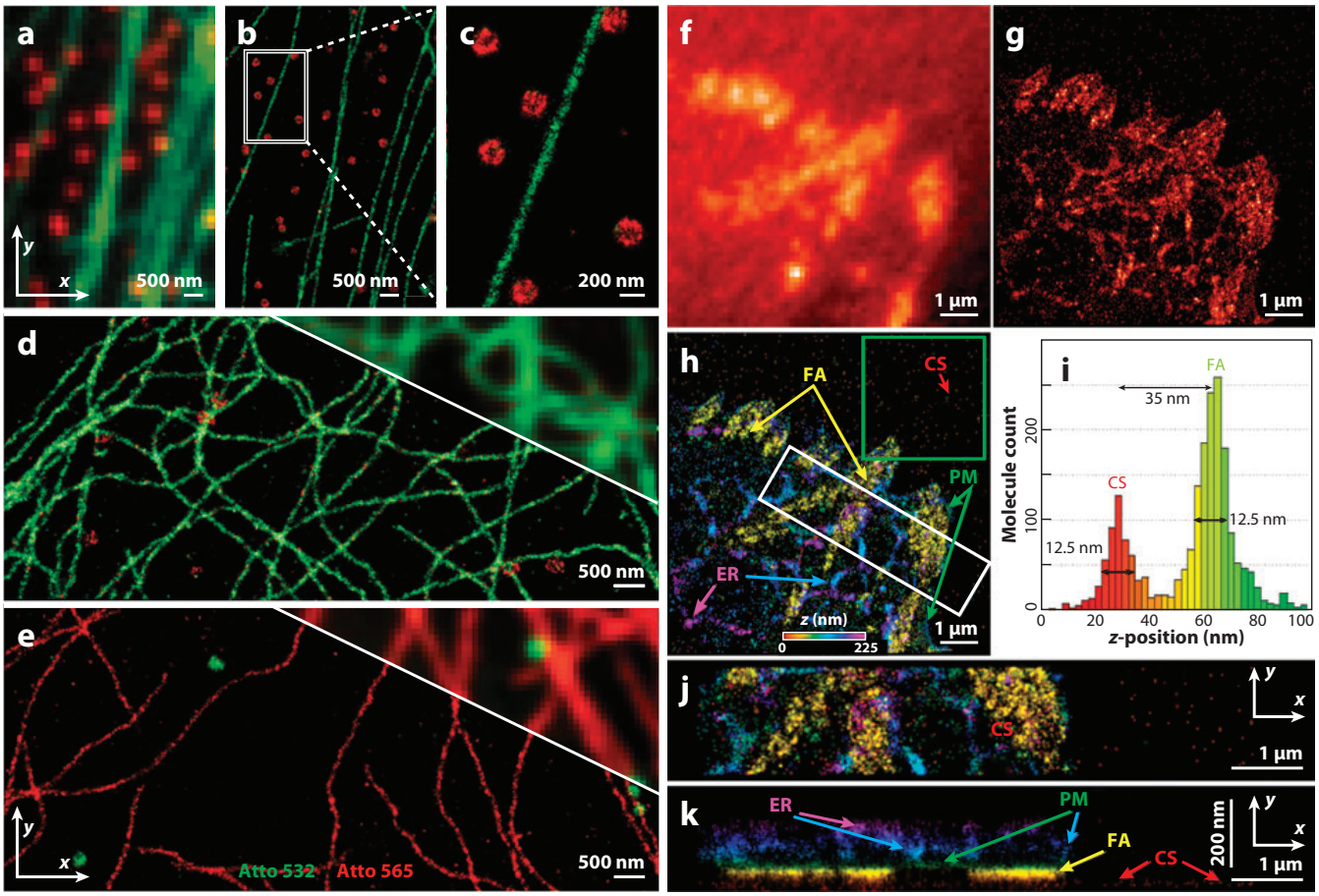

Figure 3

Examples of Pointillism microscopy. (*a–c*) Conventional (*a*) and STORM (*b*,*c*) two-color images of immunostained microtubules (*green*, Cy2-Alexa 647 pair) and clathrin-coated pits (*red*, Cy3-Alexa 647 pair) in a BSC-1 cell. The inset shown in (*b*) is magnified in (*c*). (*d*,*e*) Two-color ground-state depletion with individual molecular return (GSDIM) images of immunostained microtubules and peroxisomes of PtK2 cells embedded in polyvinyl alcohol (PVA) using conventional dyes Atto 532 (*green*) and Atto 565 (*red*). (*f–k*) iPALM data showing αV-integrin in U2OS cells genetically tagged by the photoswitchable fluorescent protein (FP) tandem dimer-EosFP, which is located in the endoplasmic reticulum (ER), the plasma membrane (PM), and focal adhesion complexes (FA) as well as on the coverslip (CS). (*f*) Wide-field image. (*g*) Two-dimensional PALM image. (*h*) Three-dimensional interferometric PALM (iPALM) image with color encoding for the axial position of each molecule, as depicted by the inset. (*i*) A *z*-position histogram of the molecules in the green box in (*h*) showing an axial resolution of at least 12.5 nm. (*j*, *k*) Magnified view of the area in the white box in (*h*) *x*-*y* and (*j*) *x*-*z* orientation (*k*). The *z*-scale is magnified by a factor of four in (*k*). (*a–c*) From Bates et al. (2007); reprinted with permission from AAAS. (*d*,*e*) Adapted with permission from Macmillan Publishers Ltd., *Nature Methods*, Fölling et al. (2008) copyright ©2008. (*f–k*) Reproduced with permission from Shtengel et al. (2009), copyright © 2009.

(**Figure 3*d*,*e***). As an alternative to fluorescent and dark state switching, binding kinetics also have been exploited to localize single bound molecules (Sharonov & Hochstrasser 2006).

Three-dimensional Pointillism. Original versions of Pointillism microscopy were limited to 2D imaging but were subsequently extended to 3D. To avoid artifacts from single molecule blinking, which causes signal fluctuations, the axial position should be obtained in a single camera frame. This problem was solved by encoding the axial position of the molecules in the lateral image.

Multiplane imaging (Prabhat et al. 2004) projects multiple focal planes from different

NanoString Exhibit 1018.013

depths of the sample onto one or more cameras. This technique simultaneously records two (or more) planes at different axial positions without axial scanning and was realized in biplane FPALM (Juette et al. 2008). The axial position of the molecule is computationally derived from the pair of images. Alternatively, a cylindrical lens in the detection path can create an oval-shaped PSF whose ellipticity is related to the axial position of the fluorophore (Huang et al. 2008b, Kao & Verkman 1994). A more complex PSF engineering technique modifies the detection PSF to resemble an axially oriented double helix (Piestun et al. 2000), which allows the axial position of every molecule to be determined from the angle between the observed foci doublets (Pavani et al. 2009b).

The achievable resolution is, interestingly, comparable between these techniques [for FPs: FWHM 20–30 nm (x, y), 50–80 nm (z)] (Mlodzianoski et al. 2009, Thompson et al. 2010). To further improve the axial resolution, Pointillism microscopy can be combined with a 4Pi microscopy/I^5M-like detection scheme at the cost of higher instrument complexity (Shtengel et al. 2009, von Middendorff et al. 2008). This interferometric PALM (iPALM) technique achieves an impressive ~25 × 25 × 10 nm 3D resolution, as shown in **Figure 3*f–k*** (Shtengel et al. 2009).

Multicolor Pointillism: challenges and solutions. As in STED microscopy, multicolor imaging is hampered because typically two different wavelengths are required per fluorophore. Moreover, fluorescence excitation light is usually orders of magnitude brighter than activation light, and accidental activation by the excitation lasers can occur. Sequential imaging with different FPs is one solution (Shroff et al. 2007, Subach et al. 2009) to this problem. Another option is to spectrally unmix spectrally similar channels (Andresen et al. 2008, Bossi et al. 2008). Using dye pairs, as first proposed in STORM (Rust et al. 2006; see **Figure 3*a–c***), a combination of three different activator dyes with three different reporter dyes provides nine different combinations for multicolor imaging (Bates et al. 2008). Although Pointillism microscopy can provide high-resolution imaging without complex hardware, its main weakness is slow speed image acquisition and extensive data postprocessing (**Table 1**).

Cellular Applications with Super-Resolution

With the emergence of super-resolution microscopes, biologists have begun to apply them. In a short period of time they have gone from imaging test objects to live specimens.

Proof of principle: seeing cellular details. Three-dimensional SIM imaging of the nucleus showed that nuclear pore complexes are adjoined by channels in both the nuclear lamin and peripheral heterochromatin (**Figure 4**; Schermelleh et al. 2008). Three-dimensional isoSTED was able to resolve the distribution of mitochondrial proteins well below the organelle level (**Figure 2*a–e***; Schmidt et al. 2008, 2009). Three-dimensional Pointillism microscopy revealed nanometer ranged contacts between mitochondria and microtubules (Huang et al. 2008a). iPALM mapped focal adhesion complexes in 3D at the highest light microscopy resolution to date (**Figure 3*f–k***; Shtengel et al. 2009). As these techniques have passed proof-of-principle tests, biologists are now applying SIM, STED microscopy, and Pointillism microscopy to a plethora of open questions that cannot be addressed with conventional light microscopy.

Structured illumination microscopy. Using SIM, researchers were able to resolve the two lateral elements of the synaptonemal complex, a central structure in meiosis, and to detect chromosomes knotted like twisted wires (Wang et al. 2009). The observation that entanglement is resolved at a late stage of meiosis indicated that the completion of synapsis requires the unknotting or snipping of these interlocks.

Annu. Rev. Cell Dev. Biol. 2010.26:285-314. Downloaded from www.annualreviews.org
by Yale University STERLING CHEMISTRY LIBRARY on 10/08/10. For personal use only.

NanoString Exhibit 1018.014

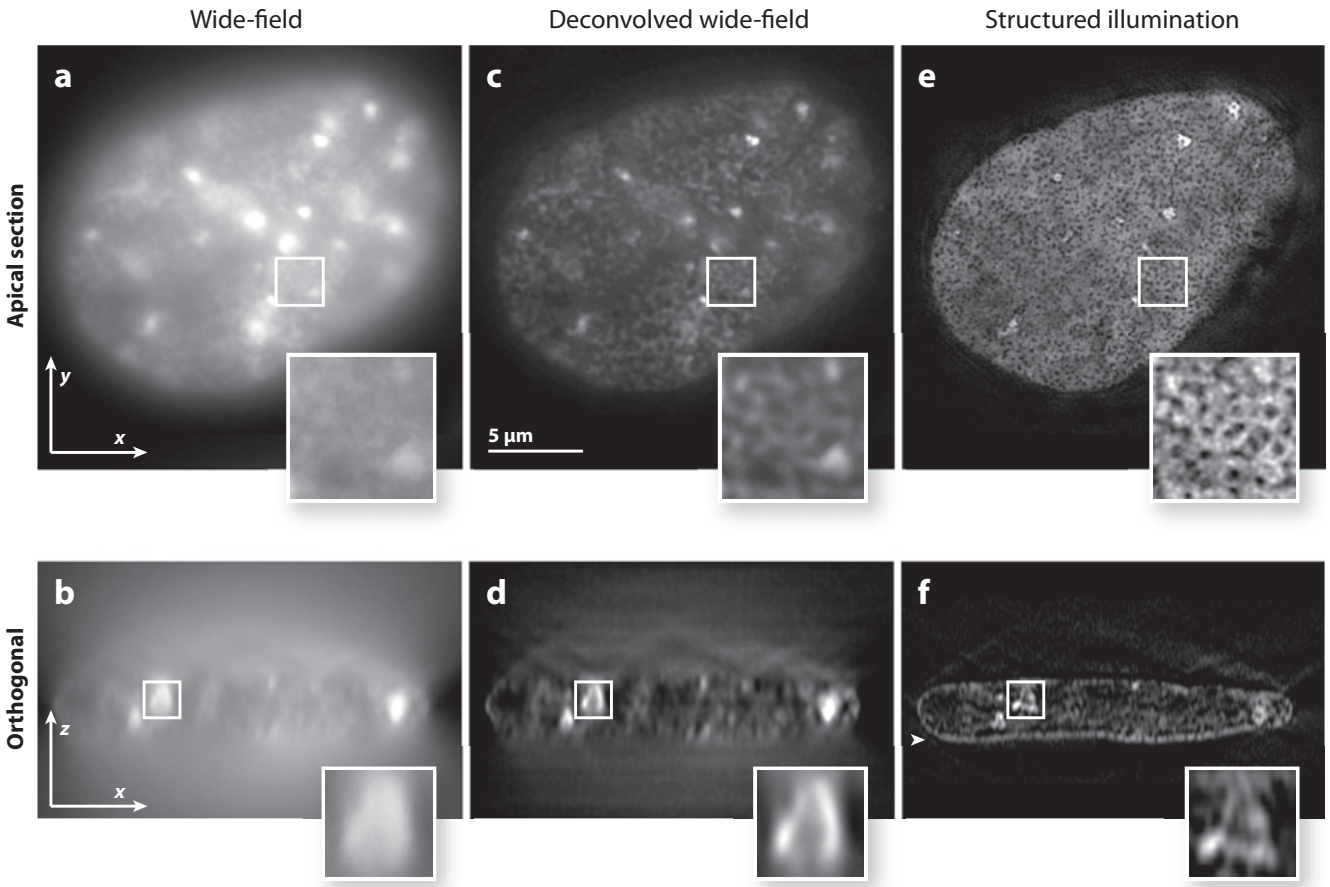

Figure 4

Wide-field images (*a*,*b*), their deconvolved variants (*c*,*d*), and structured illumination images (*e*,*f*) of the same DAPI-stained C2C12 cell nucleus. (*a*,*c*,*e*) represent the average over an apical virtual section of 500-nm thickness. Regions devoid of DAPI, which correlate with the areas near nuclear pore complexes, are resolvable for the first time with SIM (*e*). (*b*,*d*,*f*) show orthogonal virtual sections through the same nucleus. The arrowhead in (*f*) depicts the location of the apical section. The white boxes in (*a*–*f*) show the position of the magnified insets. Images from Schermelleh et al. (2008); reprinted with permission from AAAS.

Annu. Rev. Cell Dev. Biol. 2010.26:285-314. Downloaded from www.annualreviews.org
by Yale University STERLING CHEMISTRY LIBRARY on 10/08/10. For personal use only.

Stimulated emission depletion. STED has been instrumental in analyzing 50–60 nm diameter nanostructures formed by syntaxin-1 (Sieber et al. 2007). In concert with fluorescence recovery after photobleaching (FRAP) experiments and simulations, STED demonstrated that these clusters contain approximately 75 densely packed syntaxin molecules and that they exchange dynamically with a freely diffusing membrane pool. This supports protein cluster models that feature a balance between self-association and steric repulsion. STED experiments in *Drosophila* located a protein called Bruchpilot in approximately 300–500 nm large doughnut-shaped structures at the active zones of neuromuscular synapses (Kittel et al. 2006). Combined with other experiments, this indicates that Bruchpilot is involved in the organization of active zones and synaptic plasticity.

Pointillism: connecting the dots. Pointillism microscopy has been instrumental in analyzing the distribution of chemotaxis receptors in the *E. coli* cell membrane and has revealed that they are highly clustered (Greenfield et al. 2009). This cluster distribution supports the idea that stochastic self-assembly, without

NanoString Exhibit 1018.015

direct cytoskeletal involvement or active transport, is responsible for the periodic distribution of the receptors.

A twisty road toward live cell imaging. Compared with conventional microscopy, there are three major challenges in applying super-resolution microscopy to living cells: (*a*) More data (multiple frames or finer sampling in scanning) must be collected, which makes the microscopy slower. (*b*) It typically requires a higher total dose of illumination light, which can potentially harm cells. (*c*) The choice of fluorophores may be limited. Nonetheless, all three super-resolution techniques have been shown to be feasible in living cells and applied to a few selected problems, as underscored below. While the technique is still in its infancy, the potential, if these issues can be solved, is enormous.

Live structured illumination microscopy. A tricky part of SIM experiments is that all 9–15 recorded camera frames must essentially image the identical underlying structure. If the object moves during the acquisition, artifacts are created. With a judicious choice of optical components, this method is capable of 2D live cell imaging of microtubules at 11 Hz (Kner et al. 2009; see **Figure 5**).

Live stimulated emission depletion. Video-rate imaging of synaptic vesicles (28 Hz) was successfully demonstrated by streamlining the instrumentation and narrowing down the observation area to ~2.5 × 1.8 μm (Westphal et al. 2008). In this study, an organic dye (Atto 647N) was added extracellularly and endocytosed through antibodies labeling synaptotagmin. FPs, in particular Citrine, green fluorescent protein (GFP), and a tetrameric DsRed-variant, E2-Crimson, (Strack et al. 2009), were used to visualize the endoplasmic reticulum (Hein et al. 2008) and dendritic spines (Nagerl et al. 2008). STED was also combined with SNAP-tag™ (New England Biolabs) and Halotag™ (Promega) technologies; these peptide tags bind organic dyes

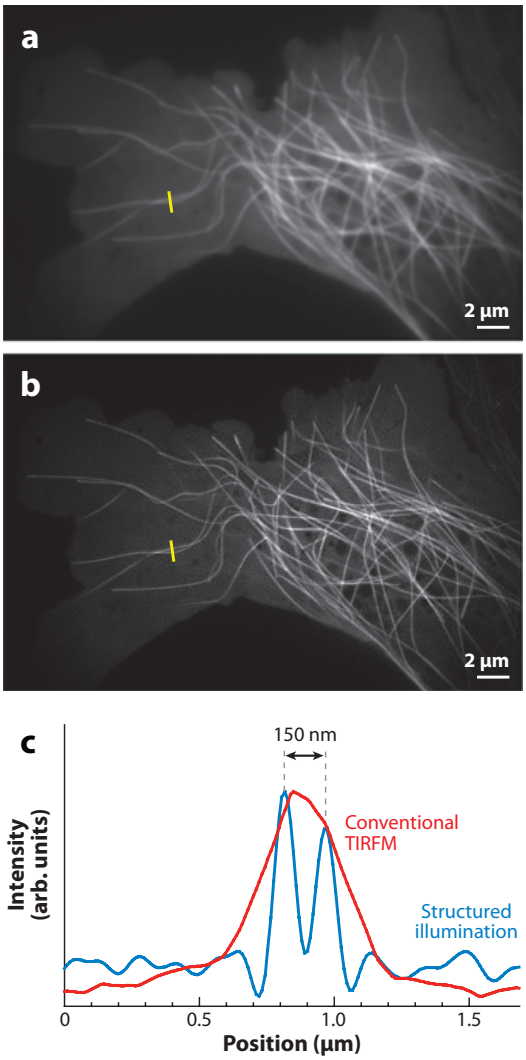

Figure 5

Example of live cell structured illumination microscopy. Microtubules (MTs) in living cells show higher lateral resolution with structured illumination-TIRFM (*b*) than with conventional TIRFM (*a*). Cross-sectional traces (*yellow*) in (*a*) and (*b*) are magnified in (*c*). Images adapted by permission from Macmillan Publishers Ltd: *Nature Methods*, Kner et al. (2009), copyright © 2009.

that are particularly well suited for STED microscopy (Hein et al. 2010, Schröder et al. 2009). The small effective spot size of STED also can be exploited to measure nanoscale dynamics in fluorescence correlation spectroscopy. This approach allowed the direct observation that sphingolipids and glycosylphosphatidylinositol-anchored proteins are trapped

Annu. Rev. Cell Dev. Biol. 2010.26:285-314. Downloaded from www.annualreviews.org
by Yale University STERLING CHEMISTRY LIBRARY on 10/08/10. For personal use only.

NanoString Exhibit 1018.016

in cholesterol-mediated sub-20 nm complexes in plasma membranes, consistent with the existence of lipid rafts or other microdomains (Eggeling et al. 2009).

Live Pointillism. Two factors must be taken into account when imaging living cells with Pointillism microscopes: (*a*) The technique requires recording 100–100,000 camera frames to acquire a single super-resolution image and hence is slow. (*b*) Most molecules can only be imaged once. Live cell Pointillism imaging, however, demonstrated that hemagglutinin was clustered in large irregular domains ranging from several tens of nanometers to micrometers wide and exhibited lateral motion of less than 200 nm (Hess et al. 2007). Other publications reported the temporal changes of proteins Gag and vesicular stomatitis virus glycoprotein (Manley et al. 2008) and the dynamics within individual adhesion complexes (Shroff et al. 2008). Following single molecules, often over multiple frames before bleaching, revealed nanofeature details as well as diffusion characteristics (Hess et al. 2007, Manley et al. 2008).

No Single Winner: Super-Resolution Trade-Offs

In **Table 1** we compare and contrast key features of the super-resolution techniques with one another and with conventional wide-field microscopy. Each technology has its strengths and limitations.

SIM requires no special specimen preparation, and identical samples can be used as for CLSM. Postacquisition image processing is required to achieve the super-resolution image. The slower temporal resolution is balanced by a gain in image resolution of approximately a factor of two in each axis (or eightfold volumetrically).

As STED is a laser scanning microscope, its imaging speed depends on the field of view. Decreasing the scanned area increases temporal resolution and can make it an excellent choice for video-rate imaging. However, the complexity of the system, especially the laser sources, limits fluorophore choices and multicolor capabilities. Recent publications have shown great promise in simplifying the instrument and increasing availability of additional laser lines (Moneron et al. 2010, Rankin & Hell 2009, Wildanger et al. 2009). STED microscopy gives immediate gratification with a what-you-see-is-what-you-get image similar to confocal microscopy and does not require data postprocessing.

Pointillism microscopes are, from an instrumentation perspective, surprisingly simple to add on to regular wide-field microscopes or TIRFM. The key lies on the choice of fluorophores as well as the proper data processing and management of large datasets, which makes its utilization trickier than conventional microscopy. However, large fields of view can be recorded easily.

Currently, only a score of serious biological applications have utilized SIM, STED microscopy, or Pointillism microscopy, with an initial emphasis on proof-of-concept studies (examples shown above). The three techniques are quite likely to establish their own application niches, as they have different strengths, but various factors must be carefully weighed. Important questions that a user wishing to use super-resolution methods should consider are: How fast is the biological process of interest? Can fixed specimens be used? How small can one crop the image? What resolution is sufficient? **Table 1** provides a guide, but the landscape is rapidly changing. Recently, many super-resolution microscopes have become commercially available, and more systems are on the horizon (see sidebar on Commercial Super-Resolution Systems).

AXIAL SUPER-RESOLUTION WITH TOTAL INTERNAL REFLECTION FLUORESCENCE MICROSCOPY

A Primer

The above super-resolution microscopes require scanning or locating sparse molecules to

Annu. Rev. Cell Dev. Biol. 2010.26:285-314. Downloaded from www.annualreviews.org
by Yale University STERLING CHEMISTRY LIBRARY on 10/08/10. For personal use only.

NanoString Exhibit 1018.017

improve axial resolution, with a commeasurable decrease in temporal resolution. TIRFM, however, uses near-field effects to achieve on-the-fly axial super-resolution (~30–100 nm; Ajo-Franklin et al. 2001) of a large field of view without scanning (see **Table 1**). Specifically, TIRFM generates a rapidly decaying evanescent field at the interface of two mediums of different refractive index (such as glass and water), which can selectively excite fluorophores in cells near the coverslip; however, it is ill suited for deep cellular imaging. Its sensitivity or signal-to-background ratio is superb, to the point that it is the method of choice for tracking single molecules in vitro and even in living cells (Axelrod 2008, Joo et al. 2008).

Despite TIRFM's early roots [pioneered by Axelrod and colleagues in the 1980s (Axelrod 2008)], the relatively recent availability of high-NA objectives and turnkey commercial systems has made TIRFM increasingly accessible and attractive to biologists, as evidenced by the outpouring of more than 500 papers using TIRFM in the past 5 years. Biologists have exploited its sensitivity to follow the cell surface dynamics of membrane trafficking, cytoskeletal remodeling, and signaling (Axelrod 2008). The old adages "seeing is believing" and "less is more" apply to TIRFM, which literally allows one to take a superficial cellular view and to see more by illuminating less. However, it also raises new challenges for interpreting what is seen, especially when observed for the first time (Simon 2009).

TIRFM is founded on the behavior of light at the interface of two mediums of different refractive index (n). When light traveling in a medium of high refractive index (n_1), such as glass, enters a lower refractive index medium (n_2), such as water, at a shallow angle of incidence (θ_1), it is refracted away from the normal (θ_2), as illustrated in **Figure 6**. The angle of refraction is governed by Snell's law: $n_1 \sin(\theta_1) = n_2 \sin(\theta_2)$. As the angle of the incident light is increased it will, at a given critical angle ($\theta_c = \sin^{-1} n_2/n_1$), exit tangentially to the interface (*blue line* in **Figure 6**). At even shallower incident angles the light will

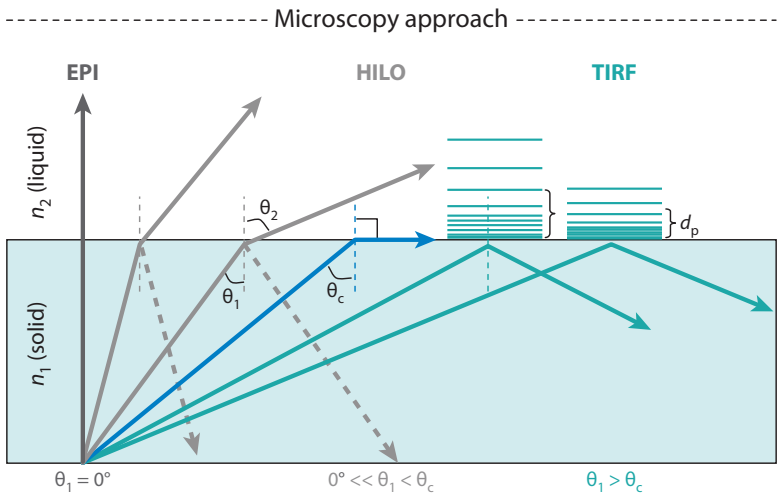

Figure 6

The diffraction and reflection of light are exploited in highly inclined laminated optical sheet (HILO) and TIRF microscopy. In TIRFM, the light is totally internally reflected (TIR) and generates an exponentially decaying evanescent wave of penetration depth d_p in the lower refractive index medium (n_2). In HILO, diffracted light (θ_2) exits at a shallow angle, whereas in epifluorescence (EPI), or regular wide-field mode, it is minimally diffracted.

undergo total internal reflection (TIR). Thus, for TIR to occur two conditions must be met: $n_1 > n_2$ and $\theta_1 > \theta_c$.

An essential feature of TIR is that the light generates a so-called evanescent wave in the lower refractive index medium (see sidebar on Common Refractive Indices) that decays exponentially in intensity away from the interface. The intensity distribution $I(z)$ of this evanescent field and its penetration depth (d_p, where the initial intensity decreases to $1/e \approx 37\%$) is dependent on the refractive indices of both mediums as well as the wavelength (λ) and angle of the incident light according to the equations:

$$I_z = I_0 e^{-z/d_p} \qquad 4.$$

and

$$d_p = \frac{\lambda}{4\pi\sqrt{n_1^2 \sin^2\theta_1 - n_2^2}}. \qquad 5.$$

A thin evanescent field can be generated by the combination of a large difference in refractive index between the two media, light of short wavelength, and a shallow angle of incident light (typically d_p is $\sim \lambda/6 - \lambda/12$) (see sidebar on Sample Total Internal Reflection

Total internal reflection (TIR): optical phenomenon by which shallow incident angle light is completely reflected at the interface with a lower refractive index medium

Annu. Rev. Cell Dev. Biol. 2010.26:285-314. Downloaded from www.annualreviews.org
by Yale University STERLING CHEMISTRY LIBRARY on 10/08/10. For personal use only.

NanoString Exhibit 1018.018

COMMERCIAL SUPER-RESOLUTION SYSTEMS

STED: Leica
PALM/STORM: Zeiss, Nikon*, Leica*
SI: Zeiss, Applied Precision, Nikon*
*announced at press time

SAMPLE TOTAL INTERNAL REFLECTION FLUORESCENCE MICROSCOPY CALCULATIONS

The critical angle θ_c and minimal penetration depth $d_{p,min}$ are used for imaging in cell cytosol at 488 nm excitation with a 1.45 NA TIRFM objective. To determine the maximum angle of light into the objective, one calculates the half aperture angle, $\alpha = \sin^{-1}(NA/n_1) = \sin^{-1}(1.45/1.51) = 73.8°$. The critical angle is determined from Snell's law, $\theta_c = \sin^{-1}1.37/1.51 = 65.1°$, and as shown, TIR occurs from 65.1° to 73.8°. The minimal penetration depth is calculated from Equation 5: $d_{p,min} = 488\ \text{nm}/4\pi(1.51^2\sin(73.8°) - 1.37^2)^{-2} = 82$ nm.

COMMON REFRACTIVE INDICES

Air = 1.00
Water = 1.33
Cell cytosol = ~1.36–1.38
Glass coverslip = 1.51

Fluorescence Microscopy Calculations). An in-depth treatment of the theoretical principles of TIRFM and role of polarization and intermediate layers can be found in an excellent treatise by Axelrod (2008).

Total Internal Reflection Fluorescence Microscopy Instrumentation

TIRFM optical setups encompass both prism-type and objective-type methods (Toomre & Axelrod 2005, Toomre & Manstein 2001), but the objective-type approach is much more widely used to image cells as it allows full access to the specimen and is sold commercially (see schematic in **Figure 7**). An essential point for cellular studies is that TIRFM is only feasible with high NA objective lenses (1.45–1.65 NA), as the NA must be greater than the refractive index of the cytosol for TIR (see sidebar on Common Refractive Indices). As shown in **Figure 7**, light is focused on the periphery of the back focal plane, which leads to an extreme angle of incidence (θ_1). One challenge is that laser light focused onto a single point can cause interference artifacts (e.g., speckles) and nonuniform illumination, both of which can be greatly decreased by annular illumination or rotating the beam in a circle (Mattheyses et al. 2006, van 't Hoff et al. 2008).

HILO: highly inclined laminated optical sheet

Seeing deeper: epifluorescence, multi-angle total internal reflection fluorescence microscopy, and highly inclined laminated optical sheet. An inherent limitation of TIRFM imaging of an object that disappears, such as an internalizing clathrin-coated pit, is that it is impossible to distinguish whether the coat dissociates or the vesicle moves inside. One solution is to alternate between TIRFM and conventional epifluorescence, using the latter to see deeper into the specimen (Merrifield et al. 2002, Saffarian & Kirchhausen 2008, Toomre et al. 2000). Another approach to axially map the positions of objects is multiangle TIRFM, which is mainly implemented on prism-type setups using a fast beam steering element to vary the incident angle between frames (Loerke et al. 2000, Stock et al. 2003). This allows a more precise tracking of the absolute position of a granule and a deeper (<0.5 μm), but still high contrast, view (Loerke et al. 2000).

However, TIRFM can be a liability, as it restricts illumination to the surface, whereas the high background of epi-illumination gives poor contrast. A new technique that takes a middle ground and can be easily performed on a TIRFM setup is highly inclined laminated optical sheet (HILO) microscopy (**Figures 6** and **7**; Tokunaga et al. 2008, van 't Hoff et al. 2008). Essentially, the laser beam is positioned at a subcritical angle on a TIRFM, which causes it to traverse the specimen as a collimated highly

Annu. Rev. Cell Dev. Biol. 2010.26:285-314. Downloaded from www.annualreviews.org
by Yale University STERLING CHEMISTRY LIBRARY on 10/08/10. For personal use only.

NanoString Exhibit 1018.019

inclined beam. This provides deep illumination with less background scatter. HILO's approximately four- to eightfold increase in signal-to-background over epi-illumination allowed the nuclear import of single GFP-importin β molecules to be visualized (Tokunaga et al. 2008).

Seeing with enhanced lateral resolution. Pointillism microscopy methods all require excellent signal-to-background ratios to map the position of single molecules. TIRFM is commonly used in 2D Pointillism microscopy to increase contrast. TIRFM can be combined with SIM to improve lateral resolution up to 2.5-fold (Chung et al. 2007, Fiolka et al. 2008, Kner et al. 2009); even higher resolution may be possible if nonlinear effects are exploited (Gustafsson 2005).

A materials-based approach to further improve lateral resolution (to ~50 nm) involves a "superlens" that refocuses the evanescent wave via patterned nanosubstrates (Fang et al. 2005). By illuminating the specimen from different directions, the near-field pattern can be moved and detected in wide-field (Sentenac et al. 2009). The lateral resolution that can be obtained here is approximately fourfold better, but could be higher (Sentenac et al. 2009). A major caveat is that special patterned nanosurfaces need to be employed, and complex nanofabrication is impractical for widespread use. However, new nanofeature stamping methods were recently reported that may make this feasible (Nagpal et al. 2009).

Seeing brighter: a silver lining to see more? Many biological imaging experiments such as fast imaging or single-molecule imaging are light starved. Interestingly, and perhaps not intuitively, the intensity of the evanescent field (I_0) can be amplified more than tenfold through surface plasmon effects using a thin (20–50 nm) metallic film (e.g., Ag, Au, Al, or Pt) on the coverslip (Axelrod 2008). These effects are highly dependent on the angle and polarization of the light and n_2 (Axelrod 2008). Dyes on the surface of the metal film are quenched, but emit photons when ~10–200 nm deeper in the aqueous medium (Lakowicz 2001). Interestingly, the near-field effects of the metal can decrease the lifetime of some dyes by an order of magnitude or more, resulting in a higher quantum efficiency (QE; and hence brightness) and greatly decreased photobleaching (Lakowicz 2001). For instance, GFP on silver island films was shown to have an approximately fourfold shorter lifetime and to emit approximately 10 times more photons before bleaching (Fu et al. 2008). Thus, there is an untapped potential to boost the signal, which can be a limiting factor in imaging of single molecule and fast dynamic cellular processes.

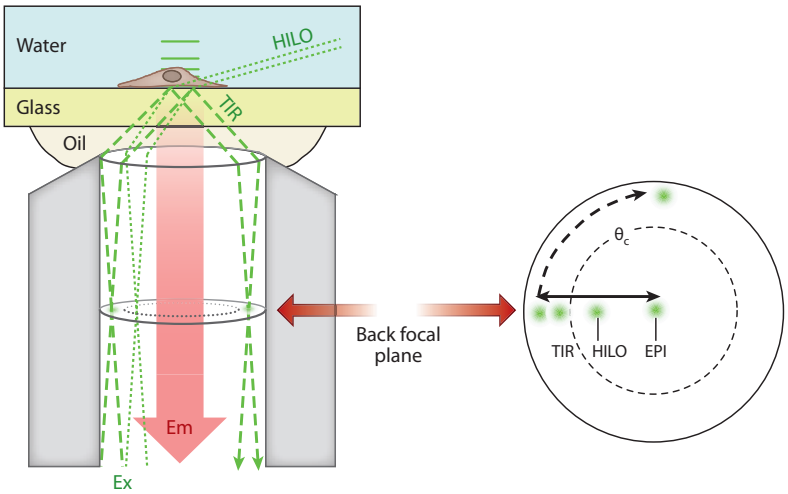

Figure 7

Objective-type TIRFM setup. Excitation light (Ex) is focused on the periphery of the back focal plane of a high-NA (1.45–1.65) objective lens. Translocation can change the incident angle of the light (and penetration depth of the evanescent field) or, when less than the critical angle (θ_c), permit HILO. Scanning the beam in a circle or semicircle can decrease interference artifacts when using laser light. Em, emitted light. Drawings are not to scale.

Cellular Applications with Total Internal Reflection Fluorescence Microscopy

TIRFM provides excellent contrast and less photobleaching (excitation is limited to a thin optical plane). This allows sharper, faster, and longer time-lapse imaging of processes near the cell surface. However, the largest impact of TIRFM is its ability to monitor fast and dynamic intermediates of organelles and

Annu. Rev. Cell Dev. Biol. 2010.26:285-314. Downloaded from www.annualreviews.org
by Yale University STERLING CHEMISTRY LIBRARY on 10/08/10. For personal use only.

NanoString Exhibit 1018.020

Annu. Rev. Cell Dev. Biol. 2010.26:285-314. Downloaded from www.annualreviews.org
by Yale University STERLING CHEMISTRY LIBRARY on 10/08/10. For personal use only.

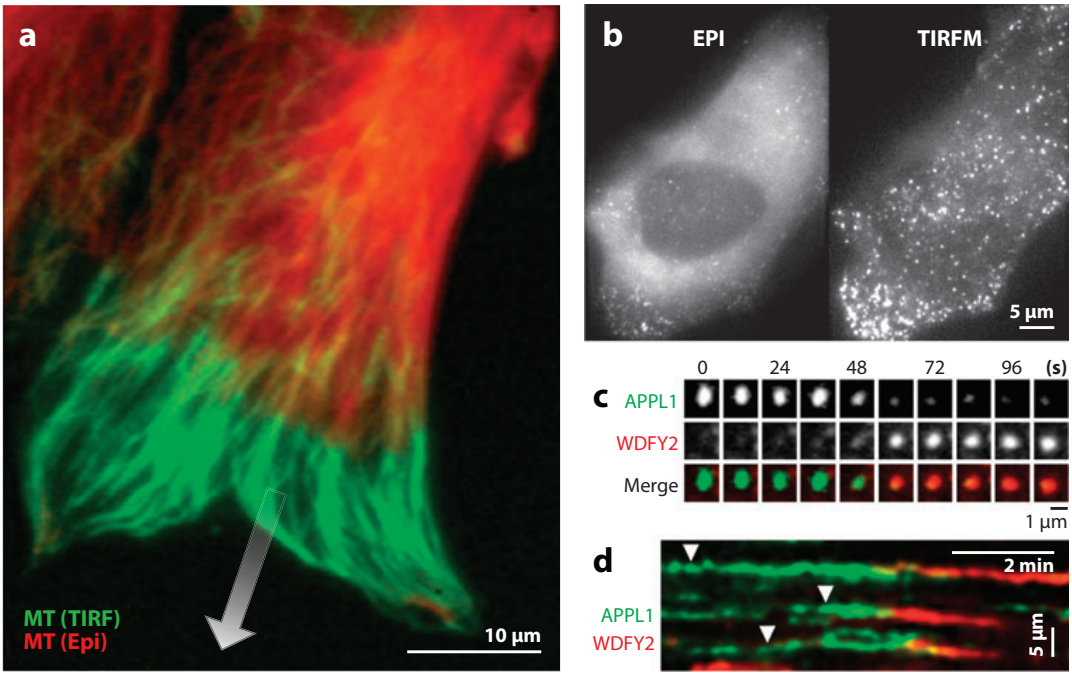

Figure 8

High-contrast TIRFM imaging of dynamic processes near the ventral surface of cells. (*a*) Microtubules on the leading edge of astrocytes that are migrating into a wound (*gray arrow*) are positioned near the cortex and are visible by TIRFM. (*b*) Gag molecules of single virons have a much higher contrast by TIRFM than by epifluorescence (EPI), which allows one to follow their assembly. (*c*,*d*) Single endosomes mature and switch from Appl1 to WDFY2, as seen by dual-color time-lapse imaging (*c*) or kymographs (*d*).
(*a*) Reprinted with permission from Etienne-Manneville et al. (2005), copyright © 2005. (*b*) Reprinted from Ivanchenko et al. (2009), copyright © 2009. (*c*,*d*) Reprinted from Zoncu et al. (2009), copyright © 2009, with permission from Elsevier.

molecules including membrane trafficking dynamics (Groves et al. 2008), cytoskeleton remodeling (Bretschneider et al. 2004), signal transduction (Weiger et al. 2009), calcium sparks (Marchaland et al. 2008), and single molecule motion and activation (Axelrod 2008, Joo et al. 2008). We focus on new discoveries and controversies that have arisen with the ability of TIRFM to visualize transient intermediates in cells. **Figures 5** and **8** show several examples of TIRFM applications.

Unraveling vesicle dynamics: kiss and tell?

Vesicle dynamics can be challenging and in some cases rife with controversy. A renowned debate concerns the presence of "kiss-and-run" vesicle fusion at the synapse (Harata et al. 2006). As the neuronal synapse's perpendicular orientation to the coverslip does not favor TIRFM [bipolar neurons are an exception (Zenisek et al. 2000)], neuroendocrine cells are often used as surrogates. TIRFM allowed researchers to directly visualize the exo-endocytic vesicle cycle. Dual color imaging of secretory cargo and membrane dyes showed that granules could release lipid probes into the membrane, or make a membrane "kiss" without fusing, in a process termed cavicapture (Taraska & Almers 2004, Tsuboi et al. 2004). Strikingly, some cargo (e.g., neuropeptide Y) was quickly released, whereas other cargoes were largely retained (Taraska et al. 2003). A partial fusion event (the kiss) was also seen in constitutive exocytosis in fibroblasts and was shown to be regulated by dynamin (Jaiswal et al. 2009, Tsuboi et al. 2004). The ability of TIRFM to peep on a vesicle's kiss should enable more extensive investigation of its regulation.

NanoString Exhibit 1018.021

Annu. Rev. Cell Dev. Biol. 2010.26:285-314. Downloaded from www.annualreviews.org
by Yale University STERLING CHEMISTRY LIBRARY on 10/08/10. For personal use only.

Membrane dynamics: seeing the ghost in the machine. In membrane trafficking of proteins and lipids, cells use diverse machinery to bud off membrane vesicles, traffic them between organelles, and fuse them with acceptor compartments; alternatively, the vesicle or organelle can mature and change its composition en route. Although many of the molecular components are known, precisely where they act and how their action is coordinated are less obvious. Simply observing the action by multicolor TIRFM (and less simply quantitating it) is extremely powerful for studying such molecular handoffs. The high contrast imaging by TIRFM can help lift the fog of background cytosolic dye, or other deeper labeling in the cell (e.g., **Figure 8*b***), to reveal dynamics near the surface. For instance, TIRFM studies of endocytosis revealed that during clathrin-coated pit internalization, dynamin suddenly appeared at a late stage, followed by subsequent recruitment of actin machinery (Merrifield et al. 2002). The former observation is consistent with dynamin acting transiently to promote fission, whereas the latter observation provided direct proof that actin is recruited to the clathrin-coated vesicle during invagination and suggests that local actin polymerization may drive internalization. In another study, epidermal growth factor trafficked through a subset of clathrin-coated pits and into a transient early endosomal compartment (APPL endosome) and in tens of seconds matured into phosphatidylinositol 3-phosphate (PI3P)-positive endosomes (Zoncu et al. 2009).

Another approach to identify changes in a vesicle's morphological state (which presumably reflects different molecular machinery) exploits the exponential decay of the evanescent field to measure small (~10 nm) axial displacements of vesicles during exocytosis and endocytosis (Karatekin et al. 2008, Saffarian & Kirchhausen 2008). For instance, granules were observed making a 20 nm axial jump toward the membrane just before fusion, which suggested a change from a more distant tethered state to a closer docked state (Karatekin et al. 2008). In a separate study, vesicles were reported to make a lateral (*xy*) shift just before fusion, suggesting that docking and priming (a step that prepares vesicles for release) are not stable processes (Degtyar et al. 2007); however, a separate study indicated that vesicle priming represents a nearly immobile state (Nofal et al. 2007). Unfortunately, nomenclature and analysis, which are operationally defined and not standardized, make it even more difficult to cross-compare studies and their apparently conflicting, yet tantalizing, results. Nevertheless, TIRFM's ability to characterize these processes represents the first step in elucidating a vesicle's last steps.

Act locally and globally. Tracking the motion of individual motors and organelles in cell division and cytokinesis is extremely difficult because of high background noise from the cytoplasm. Although the cleavage furrow is normally strung like a suspension bridge between the daughter cells, in cases in which it is either fortuitously or artificially anchored to the glass, it can be seen with remarkable clarity by TIRFM. For instance, both daughter cells spatially directed constitutive membrane traffic to the furrow (Goss & Toomre 2008). In terms of molecular motors, Kinesin-6 relocalized to the tips of a subset of stable microtubules that grow into the cortex of anaphase cells (Vale et al. 2009). Concomitantly, myosin rapidly assembled de novo at the midbody, rather than exclusively by cortical flow (Vale et al. 2009, Yumura et al. 2008, Zhou & Wang 2008). These new observations challenge the previous hypothesis of global contraction by polar relaxation and suggest that there is local regulation at the midbody, including integration of multiple inputs, rather than purely global action.

Getting the cellular move on. Cell migration requires a tight coordination of signal transduction, cytoskeleton remodeling, and membrane traffic. TIRFM has facilitated visualization of the signaling pathways that lead to cell migration. For instance, spontaneous PI3K signaling in fibroblasts was activated at membrane protrusions during cell migration (Weiger et al. 2009). Microtubules plus end tips can target

NanoString Exhibit 1018.022

focal adhesions in the cortex (Krylyshkina et al. 2003) and, in migrating astrocytes, are spatially targeted via adenomatous polyposis coli (APC) and Dlg1 through Cdc42-activated Par6-PKCζ at the leading edge (Etienne-Manneville & Hall 2003, Etienne-Manneville et al. 2005). Microtubules and exocyst-tethering machinery are also required for polarized fusion of vesicles at the leading edge (Letinic et al. 2009, Schmoranzer et al. 2003).

Whereas observing molecules in cells is useful, controlling their interactions (while watching) is even better. Recently, several new strategies have been developed in which photoactivating light can drive dimerization and recruitment of proteins (e.g., Rac or Rho GTPases) to the surface, where their recruitment and effect on lamellipodia formation were seen by TIRFM (Levskaya et al. 2009, Yazawa et al. 2009).

Virus invasion, assembly, and departure. Pathogens are adept at hijacking cellular machinery to enter and leave cells, and TIRFM is an excellent tool to view viral entry, internal assembly, and exocytosis. There are many ways in: SV40 virus use caveolae to enter cells (Tagawa et al. 2005), whereas HIV Nef-1 enters through clathrin-coated pits (Burtey et al. 2007). Using TIRFM imaging of a tagged Gag, a major structural component of HIV, viral assembly was nucleated at the plasma membrane surface in only 5–9 min, whereas viral release required approximately 30 min and could be detected by an increase in lateral motility or pH sensitivity (Ivanchenko et al. 2009, Jouvenet et al. 2008).

Seeing single molecules in action. In vitro, polarized TIRFM allowed myosin VI's trajectory to be followed in 3D with nanometer localization precision and revealed a highly variable working stroke and a "wiggly walk" (Sun et al. 2007, Toprak et al. 2006). TIRFM sensitivity has also allowed investigators to track the movement of single myosin and kinesin motors in living cells (Cai et al. 2007, Kerber et al. 2009) and even to detect epidermal growth factor dimerization by fluoresence resonance energy transfer (FRET) (Sako et al. 2000). Due to the dim signal, tracking single GFP-tagged molecules in cells is challenging and requires careful controls (Mashanov & Molloy 2007, Wennmalm & Simon 2007); even so, looking evanescently is bringing single molecules into the limelight.

LOOKING BACK AND PROJECTING FORWARD

Why is there a major push on super-resolution imaging now and not earlier? TIRFM was first realized only two decades ago (Campanella et al. 1988), and Stefan Hell's seminal STED paper (Hell & Wichmann 1994) was published 16 years ago. The rising new wave is, in our opinion, due to both a conceptual and technological shift. Conceptually, leaders in the field pushed special cases in which Abbe's resolution limit no longer applied, namely near field excitation (TIRFM), targeted optical switching by nonlinear effects (STED or RESOLFT), and stochastic switching and localization of sparse single molecules (Pointillism microscopy). Their success caused a paradigm shift, and the question is no longer if Abbe's limit can be broken, but by how much?

Parallel technological advances in other fields played an equally crucial role. Powerful lasers and sensitive detectors enabled STED. (F)PALM and STORM were realized with photoactivatable FPs and the photoswitching of pairs of cyanine dyes, respectively. Single molecule detection was facilitated by better cameras [e.g., electron-multiplying charge coupled devices (EMCCDs)], whereas modern computers allow hundreds of gigabytes of data to be stored and millions of single molecules to be detected automatically. In TIRFM, the GFP revolution greatly expanded cellular imaging, and commercial systems dropped the do-it-yourself entry barrier.

We project that new technologies will continue to enable rapid growth of biological imaging. Recently announced new "scientific CMOS (complementary metal–oxide–semiconductor)" cameras have high

Annu. Rev. Cell Dev. Biol. 2010.26:285-314. Downloaded from www.annualreviews.org
by Yale University STERLING CHEMISTRY LIBRARY on 10/08/10. For personal use only.

NanoString Exhibit 1018.023

sensitivity (<2 electron read noise), efficiency (~60% QE), and large size (5.5 megapixels) and can acquire full-chip images at up to 100 Hz. However, they will quickly fill up hard drives unless there are parallel advances in data storage and analysis. Graphics processing units (GPUs) on computer video cards are inexpensive and can process 150 gigaflops—more than a supercomputer of the mid-1990s. Recently, GPUs have been shown to accelerate data processing in Pointillism microscopy significantly (Smith et al. 2010). As many super-resolution approaches rely on the switching of fluorophores between two states (e.g., ground/excited, dark/light), advances in designer FPs and chemical dyes will be crucial; ideal dyes here may be derivatives of former dyes that were inappropriate for ensemble studies (e.g., good photophysical properties, but largely in the dark state).

But is super-resolution microscopy just in vogue or truly a new wave? The new nanoscopes are still in their early days, and we contend that super-resolution microscopy is a rising new wave, but it will be increasingly important to take it to living cells in multicolor and 3D as well as into the hands of more biologists. If TIRFM is an indicator, the applications will follow. The greatest impact will likely occur in areas in which one desparately needs to see more details in live cells, such as the dense organization in the nucleus and synapse. The recent commercialization of all categories of super-resolution approaches will help. At the leading edge, video-rate imaging by STED microscopy and iPALM resolution between 10 and 25 nm in 3D show great promise, but a subsecond 10 μm^3 super-resolution system with tens of nanometers resolution has yet to be achieved. As future predictions are often wrong, especially when based on tomorrow's technologies, perhaps it is as Alan Kay (1989) prophesized: "The best way to predict the future is to invent it." Today's super-resolution pioneers are doing just that.

SUMMARY POINTS

No single super-resolution system is ideal. All have their separate advantages and limitations and should be carefully selected for the biological problem at hand (see **Table 1** for a comparison of their pros and cons).

STED (generalized by RESOLFT methods) and Pointillism nanoscopy rely on switching fluorophores between two different states.

TIRFM yields superaxial resolution and high contrast by generation of an exponentially decaying evanescent wave.

Higher resolution imaging requires a labeling density of structures of interest higher than the resolution level to avoid random signal gaps in the observed structures.

An increase in spatial resolution is generally achieved at a decrease in temporal resolution because finer sampling is required either by a higher density of detected probes (Pointillism) or by smaller scanning steps (SIM and STED). This also holds true for TIRFM when depth information needs to be obtained (multiangle TIRFM).

FUTURE ISSUES

The improvement of FPs and chemical dyes that can switch between states will enhance current super-resolution methods.

Brighter and more photostable probes would enhance tracking of single molecules inside cells.

Annu. Rev. Cell Dev. Biol. 2010.26:285-314. Downloaded from www.annualreviews.org
by Yale University STERLING CHEMISTRY LIBRARY on 10/08/10. For personal use only.

NanoString Exhibit 1018.024

Robust and user-friendly image processing and data mining tools are required for quantitative measurements and modeling.

Major advances will require a concerted interdisciplinary effort from scientists in physics, optics, chemistry, biology, materials science, and computer science.

DISCLOSURE STATEMENT

D.T. holds patents for the development of novel TIRFM illumination optics. J.B. holds patents for developments related to the field discussed in this article.

ACKNOWLEDGMENTS

D.T. was supported by an NIH New Innovator Award. We thank Patrick Lusk, Michael W. Davidson, Alexander Karpikov, and Ann Haberman for their detailed comments and suggestions.

LITERATURE CITED

Abbe E. 1873. Beiträge zur Theorie des Mikroskops und der mikroskopischen Wahrnehmung. *Arch. Mikr. Anat.* 9:413–68

Ajo-Franklin CM, Kam L, Boxer SG. 2001. High refractive index substrates for fluorescence microscopy of biological interfaces with high *z* contrast. *Proc. Natl. Acad. Sci. USA* 98:13643–48

Andresen M, Stiel AC, Fölling J, Wenzel D, Schönle A, et al. 2008. Photoswitchable fluorescent proteins enable monochromatic multilabel imaging and dual color fluorescence nanoscopy. *Nat. Biotechnol.* 26:1035–40

Axelrod D. 2008. Chapter 7: Total internal reflection fluorescence microscopy. *Methods Cell Biol.* 89:169–221

Baddeley D, Jayasinghe ID, Cremer C, Cannell MB, Soeller C. 2009. Light-induced dark states of organic fluochromes enable 30 nm resolution imaging in standard media. *Biophys. J.* 96:L22–24

Bates M, Huang B, Dempsey GT, Zhuang X. 2007. Multicolor super-resolution imaging with photoswitchable fluorescent probes. *Science* 317:1749–53

Bates M, Huang B, Zhuang X. 2008. Super-resolution microscopy by nanoscale localization of photoswitchable fluorescent probes. *Curr. Opin. Chem. Biol.* 12:505–14

Betzig E, Patterson GH, Sougrat R, Lindwasser OW, Olenych S, et al. 2006. Imaging intracellular fluorescent proteins at nanometer resolution. *Science* 313:1642–45

Bewersdorf J, Schmidt R, Hell SW. 2006. Comparison of I^5M and 4Pi-microscopy. *J. Microsc.* 222:105–17

Bossi M, Belov V, Polyakova S, Hell SW. 2006. Reversible red fluorescent molecular switches. *Angew. Chem. Int. Ed.* 45:7462–65

Bossi M, Fölling J, Belov VN, Boyarskiy VP, Medda R, et al. 2008. Multicolor far-field fluorescence nanoscopy through isolated detection of distinct molecular species. *Nano Lett.* 8:2463–68

Bretschneider T, Diez S, Anderson K, Heuser J, Clarke M, et al. 2004. Dynamic actin patterns and Arp2/3 assembly at the substrate-attached surface of motile cells. *Curr. Biol.* 14:1–10

Bretschneider S, Eggeling C, Hell SW. 2007. Breaking the diffraction barrier in fluorescence microscopy by optical shelving. *Phys. Rev. Lett.* 98:218103

Burtey A, Rappoport JZ, Bouchet J, Basmaciogullari S, Guatelli J, et al. 2007. Dynamic interaction of HIV-1 Nef with the clathrin-mediated endocytic pathway at the plasma membrane. *Traffic* 8:61–76

Cai D, Verhey KJ, Meyhöfer E. 2007. Tracking single kinesin molecules in the cytoplasm of mammalian cells. *Biophys. J.* 92:4137–44

Campanella C, Talevi R, Kline D, Nuccitelli R. 1988. The cortical reaction in the egg of *Discoglossus pictus*: a study of the changes in the endoplasmic reticulum at activation. *Dev. Biol.* 130:108–19

Chudakov DM, Verkhusha VV, Staroverov DB, Souslova EA, Lukyanov S, Lukyanov KA. 2004. Photoswitchable cyan fluorescent protein for protein tracking. *Nat. Biotechnol.* 22:1435–39

Annu. Rev. Cell Dev. Biol. 2010.26:285-314. Downloaded from www.annualreviews.org
by Yale University STERLING CHEMISTRY LIBRARY on 10/08/10. For personal use only.

NanoString Exhibit 1018.025

Chung E, Kim D, Cui Y, Kim YH, So PT. 2007. Two-dimensional standing wave total internal reflection fluorescence microscopy: superresolution imaging of single molecular and biological specimens. *Biophys. J.* 93:1747–57

Conley NR, Biteen JS, Moerner WE. 2008. Cy3-Cy5 covalent heterodimers for single-molecule photoswitching. *J. Phys. Chem. B* 112:11878–80

Degtyar VE, Allersma MW, Axelrod D, Holz RW. 2007. Increased motion and travel, rather than stable docking, characterize the last moments before secretory granule fusion. *Proc. Natl. Acad. Sci. USA* 104:15929–34

Dunn KW, Sutton TA. 2008. Functional studies in living animals using multiphoton microscopy. *ILAR J.* 49:66–77

Dyba M, Hell SW. 2002. Focal spots of size λ/23 open up far-field fluorescence microscopy at 33 nm axial resolution. *Phys. Rev. Lett.* 88:163901

Eggeling C, Ringemann C, Medda R, Schwarzmann G, Sandhoff K, et al. 2009. Direct observation of the nanoscale dynamics of membrane lipids in a living cell. *Nature* 457:1159–62

Egner A, Geisler C, von Middendorff C, Bock H, Wenzel D, et al. 2007. Fluorescence nanoscopy in whole cells by asynchronous localization of photoswitching emitters. *Biophys. J.* 93:3285–90

Etienne-Manneville S, Hall A. 2003. Cdc42 regulates GSK-3β and adenomatous polyposis coli to control cell polarity. *Nature* 421:753–56

Etienne-Manneville S, Manneville JB, Nicholls S, Ferenczi MA, Hall A. 2005. Cdc42 and Par6-PKCζ regulate the spatially localized association of Dlg1 and APC to control cell polarization. *J. Cell Biol.* 170:895–901

Fang N, Lee H, Sun C, Zhang X. 2005. Sub-diffraction-limited optical imaging with a silver superlens. *Science* 308:534–37

Fernandez-Suarez M, Ting AY. 2008. Fluorescent probes for super-resolution imaging in living cells. *Nat. Rev. Mol. Cell Biol.* 9:929–43

Fiolka R, Beck M, Stemmer A. 2008. Structured illumination in total internal reflection fluorescence microscopy using a spatial light modulator. *Opt. Lett.* 33:1629–31

Fölling J, Bossi M, Bock H, Medda R, Wurm CA, et al. 2008. Fluorescence nanoscopy by ground-state depletion and single-molecule return. *Nat. Methods* 5:943–45

Fu Y, Zhang J, Lakowicz JR. 2008. Metal-enhanced fluorescence of single green fluorescent protein (GFP). *Biochem. Biophys. Res. Commun.* 376:712–17

Gelles J, Schnapp BJ, Sheetz MP. 1988. Tracking kinesin-driven movements with nanometre-scale precision. *Nature* 331:450–53

Gordon MP, Ha T, Selvin PR. 2004. Single-molecule high-resolution imaging with photobleaching. *Proc. Natl. Acad. Sci. USA* 101:6462–65

Goss JW, Toomre DK. 2008. Both daughter cells traffic and exocytose membrane at the cleavage furrow during mammalian cytokinesis. *J. Cell Biol.* 181:1047–54

Greenfield D, McEvoy AL, Shroff H, Crooks GE, Wingreen NS, et al. 2009. Self-organization of the *Escherichia coli* chemotaxis network imaged with super-resolution light microscopy. *PLoS Biol.* 7:e1000137

Groves JT, Parthasarathy R, Forstner MB. 2008. Fluorescence imaging of membrane dynamics. *Annu. Rev. Biomed. Eng.* 10:311–38

Gugel H, Bewersdorf J, Jakobs S, Engelhardt J, Storz R, Hell SW. 2004. Cooperative 4Pi excitation and detection yields sevenfold sharper optical sections in live-cell microscopy. *Biophys. J.* 87:4146–52

Gurskaya NG, Verkhusha VV, Shcheglov AS, Staroverov DB, Chepurnykh TV, et al. 2006. Engineering of a monomeric green-to-red photoactivatable fluorescent protein induced by blue light. *Nat. Biotechnol.* 24:461–65

Gustafsson MG. 2000. Surpassing the lateral resolution limit by a factor of two using structured illumination microscopy. *J. Microsc.* 198:82–87

Gustafsson MG. 2005. Nonlinear structured-illumination microscopy: wide-field fluorescence imaging with theoretically unlimited resolution. *Proc. Natl. Acad. Sci. USA* 102:13081–86

Gustafsson MG. 2008. Super-resolution light microscopy goes live. *Nat. Methods* 5:385–87

Gustafsson MG, Agard DA, Sedat JW. 1999. I5M: 3D widefield light microscopy with better than 100 nm axial resolution. *J. Microsc.* 195:10–16

Annu. Rev. Cell Dev. Biol. 2010.26:285-314. Downloaded from www.annualreviews.org
by Yale University STERLING CHEMISTRY LIBRARY on 10/08/10. For personal use only.

NanoString Exhibit 1018.026

Gustafsson MG, Shao L, Carlton PM, Wang CJ, Golubovskaya IN, et al. 2008. Three-dimensional resolution doubling in wide-field fluorescence microscopy by structured illumination. *Biophys. J.* 94:4957–70

Harata NC, Aravanis AM, Tsien RW. 2006. Kiss-and-run and full-collapse fusion as modes of exo-endocytosis in neurosecretion. *J. Neurochem.* 97:1546–70

Harke B, Keller J, Ullal CK, Westphal V, Schönle A, Hell SW. 2008a. Resolution scaling in STED microscopy. *Opt. Express* 16:4154–62

Harke B, Ullal CK, Keller J, Hell SW. 2008b. Three-dimensional nanoscopy of colloidal crystals. *Nano Lett.* 8:1309–13

Heilemann M, van de Linde S, Schuttpelz M, Kasper R, Seefeldt B, et al. 2008. Subdiffraction-resolution fluorescence imaging with conventional fluorescent probes. *Angew. Chem. Int. Ed.* 47:6172–76

Hein B, Willig KI, Hell SW. 2008. Stimulated emission depletion (STED) nanoscopy of a fluorescent protein-labeled organelle inside a living cell. *Proc. Natl. Acad. Sci. USA* 105:14271–76

Hein B, Willig KI, Wurm CA, Westphal V, Jakobs S, Hell SW. 2010. Stimulated emission depletion nanoscopy of living cells using SNAP-tag fusion proteins. *Biophys. J.* 98:158–63

Heintzmann R, Jovin TM, Cremer C. 2002. Saturated patterned excitation microscopy—a concept for optical resolution improvement. *J. Opt. Soc. Am. A* 19:1599–609

Hell S, Stelzer EHK. 1992. Fundamental improvement of resolution with a 4Pi-confocal fluorescence microscope using two-photon excitation. *Opt. Commun.* 93:277–82

Hell SW. 2003. Toward fluorescence nanoscopy. *Nat. Biotechnol.* 21:1347–55

Hell SW. 2007. Far-field optical nanoscopy. *Science* 316:1153–58

Hell SW, Kroug M. 1995. Ground-state-depletion fluorescence microscopy: a concept for breaking the diffraction resolution limit. *Appl. Phys. B* 60:495–97

Hell SW, Wichmann J. 1994. Breaking the diffraction resolution limit by stimulated emission: stimulated-emission-depletion fluorescence microscopy. *Opt. Lett.* 19:780–82

Hess ST, Girirajan TP, Mason MD. 2006. Ultra-high resolution imaging by fluorescence photoactivation localization microscopy. *Biophys. J.* 91:4258–72

Hess ST, Gould TJ, Gudheti MV, Maas SA, Mills KD, Zimmerberg J. 2007. Dynamic clustered distribution of hemagglutinin resolved at 40 nm in living cell membranes discriminates between raft theories. *Proc. Natl. Acad. Sci. USA* 104:17370–75

Hofmann M, Eggeling C, Jakobs S, Hell SW. 2005. Breaking the diffraction barrier in fluorescence microscopy at low light intensities by using reversibly photoswitchable proteins. *Proc. Natl. Acad. Sci. USA* 102:17565–69

Huang B, Bates M, Zhuang X. 2009. Super-resolution fluorescence microscopy. *Annu. Rev. Biochem.* 78:993–1016

Huang B, Jones SA, Brandenburg B, Zhuang X. 2008a. Whole-cell 3D STORM reveals interactions between cellular structures with nanometer-scale resolution. *Nat. Methods* 5:1047–52

Huang B, Wang W, Bates M, Zhuang X. 2008b. Three-dimensional super-resolution imaging by stochastic optical reconstruction microscopy. *Science* 319:810–13

Irvine SE, Staudt T, Rittweger E, Engelhardt J, Hell SW. 2008. Direct light-driven modulation of luminescence from Mn-doped ZnSe quantum dots. *Angew. Chem. Int. Ed.* 47:2685–88

Ivanchenko S, Godinez WJ, Lampe M, Krausslich HG, Eils R, et al. 2009. Dynamics of HIV-1 assembly and release. *PLoS Pathog.* 5:e1000652

Jaiswal JK, Rivera VM, Simon SM. 2009. Exocytosis of post-Golgi vesicles is regulated by components of the endocytic machinery. *Cell* 137:1308–19

Joo C, Balci H, Ishitsuka Y, Buranachai C, Ha T. 2008. Advances in single-molecule fluorescence methods for molecular biology. *Annu. Rev. Biochem.* 77:51–76

Jouvenet N, Bieniasz PD, Simon SM. 2008. Imaging the biogenesis of individual HIV-1 virions in live cells. *Nature* 454:236–40

Juette MF, Gould TJ, Lessard MD, Mlodzianoski MJ, Nagpure BS, et al. 2008. Three-dimensional sub-100 nm resolution fluorescence microscopy of thick samples. *Nat. Methods* 5:527–29

Kao HP, Verkman AS. 1994. Tracking of single fluorescent particles in three dimensions: use of cylindrical optics to encode particle position. *Biophys. J.* 67:1291–300

Annu. Rev. Cell Dev. Biol. 2010.26:285-314. Downloaded from www.annualreviews.org
by Yale University STERLING CHEMISTRY LIBRARY on 10/08/10. For personal use only.

NanoString Exhibit 1018.027

Karatekin E, Tran VS, Huet S, Fanget I, Cribier S, Henry JP. 2008. A 20-nm step toward the cell membrane preceding exocytosis may correspond to docking of tethered granules. *Biophys. J.* 94:2891–905

Kay AC. 1989. Predicting the future. *Stanford Engineering* 1(1):1–6

Keller PJ, Schmidt AD, Wittbrodt J, Stelzer EH. 2008. Reconstruction of zebrafish early embryonic development by scanned light sheet microscopy. *Science* 322:1065–69

Kerber ML, Jacobs DT, Campagnola L, Dunn BD, Yin T, et al. 2009. A novel form of motility in filopodia revealed by imaging myosin-X at the single-molecule level. *Curr. Biol.* 19:967–73

Kittel RJ, Wichmann C, Rasse TM, Fouquet W, Schmidt M, et al. 2006. Bruchpilot promotes active zone assembly, Ca^{2+} channel clustering, and vesicle release. *Science* 312:1051–54

Klar TA, Jakobs S, Dyba M, Egner A, Hell SW. 2000. Fluorescence microscopy with diffraction resolution barrier broken by stimulated emission. *Proc. Natl. Acad. Sci. USA* 97:8206–10

Kner P, Chhun BB, Griffis ER, Winoto L, Gustafsson MG. 2009. Super-resolution video microscopy of live cells by structured illumination. *Nat. Methods* 6:339–42

Krylyshkina O, Anderson KI, Kaverina I, Upmann I, Manstein DJ, et al. 2003. Nanometer targeting of microtubules to focal adhesions. *J. Cell Biol.* 161:853–59

Lakowicz JR. 2001. Radiative decay engineering: biophysical and biomedical applications. *Anal. Biochem.* 298:1–24

Letinic K, Sebastian R, Toomre D, Rakic P. 2009. Exocyst is involved in polarized cell migration and cerebral cortical development. *Proc. Natl. Acad. Sci. USA* 106:11342–47

Levskaya A, Weiner OD, Lim WA, Voigt CA. 2009. Spatiotemporal control of cell signaling using a light-switchable protein interaction. *Nature* 461:997–1001

Lidke K, Rieger B, Jovin T, Heintzmann R. 2005. Superresolution by localization of quantum dots using blinking statistics. *Opt. Express* 13:7052–62

Loerke D, Preitz B, Stuhmer W, Oheim M. 2000. Super-resolution measurements with evanescent-wave fluorescence excitation using variable beam incidence. *J. Biomed. Opt.* 5:23–30

Manley S, Gillette JM, Patterson GH, Shroff H, Hess HF, et al. 2008. High-density mapping of single-molecule trajectories with photoactivated localization microscopy. *Nat. Methods* 5:155–57

Marchaland J, Cali C, Voglmaier SM, Li H, Regazzi R, et al. 2008. Fast subplasma membrane Ca^{2+} transients control exo-endocytosis of synaptic-like microvesicles in astrocytes. *J. Neurosci.* 28:9122–32

Mashanov GI, Molloy JE. 2007. Automatic detection of single fluorophores in live cells. *Biophys. J.* 92:2199–211

Mattheyses AL, Shaw K, Axelrod D. 2006. Effective elimination of laser interference fringing in fluorescence microscopy by spinning azimuthal incidence angle. *Microsc. Res. Tech.* 69:642–47

McKinney SA, Murphy CS, Hazelwood KL, Davidson MW, Looger LL. 2009. A bright and photostable photoconvertible fluorescent protein. *Nat. Methods* 6:131–33

McNally JG, Karpova T, Cooper J, Conchello JA. 1999. Three-dimensional imaging by deconvolution microscopy. *Methods* 19:373–85

Merrifield CJ, Feldman ME, Wan L, Almers W. 2002. Imaging actin and dynamin recruitment during invagination of single clathrin-coated pits. *Nat. Cell Biol.* 4:691–98

Meyer L, Wildanger D, Medda R, Punge A, Rizzoli SO, et al. 2008. Dual-color STED microscopy at 30-nm focal-plane resolution. *Small* 4:1095–100

Mlodzianoski MJ, Juette MF, Beane GL, Bewersdorf J. 2009. Experimental characterization of 3D localization techniques for particle-tracking and super-resolution microscopy. *Opt. Express* 17:8264–77

Moneron G, Medda R, Hein B, Giske A, Westphal V, Hell SW. 2010. Fast STED microscopy with continuous wave fiber lasers. *Opt. Express* 18:1302–9

Nagerl UV, Willig KI, Hein B, Hell SW, Bonhoeffer T. 2008. Live-cell imaging of dendritic spines by STED microscopy. *Proc. Natl. Acad. Sci. USA* 105:18982–87

Nagpal P, Lindquist NC, Oh SH, Norris DJ. 2009. Ultrasmooth patterned metals for plasmonics and metamaterials. *Science* 325:594–97

Nofal S, Becherer U, Hof D, Matti U, Rettig J. 2007. Primed vesicles can be distinguished from docked vesicles by analyzing their mobility. *J. Neurosci.* 27:1386–95

Patterson G, Davidson M, Manley S, Lippincott-Schwartz J. 2010. Superresolution imaging using single-molecule localization. *Annu. Rev. Phys. Chem.* 61:345–67

Annu. Rev. Cell Dev. Biol. 2010.26:285-314. Downloaded from www.annualreviews.org
by Yale University STERLING CHEMISTRY LIBRARY on 10/08/10. For personal use only.

NanoString Exhibit 1018.028

Patterson GH, Lippincott-Schwartz J. 2002. A photoactivatable GFP for selective photolabeling of proteins and cells. *Science* 297:1873–77

Pavani SR, DeLuca JG, Piestun R. 2009a. Polarization sensitive, three-dimensional, single-molecule imaging of cells with a double-helix system. *Opt. Express* 17:19644–55

Pavani SR, Thompson MA, Biteen JS, Lord SJ, Liu N, et al. 2009b. Three-dimensional, single-molecule fluorescence imaging beyond the diffraction limit by using a double-helix point spread function. *Proc. Natl. Acad. Sci. USA* 106:2995–99

Pawley JB, ed. 2005. *Handbook of Biological Confocal Microscopy*. New York: Plenum

Piestun R, Schechner YY, Shamir J. 2000. Propagation-invariant wave fields with finite energy. *J. Opt. Soc. Am. A* 17:294–303

Prabhat P, Ram S, Ward ES, Ober RJ. 2004. Simultaneous imaging of different focal planes in fluorescence microscopy for the study of cellular dynamics in three dimensions. *IEEE Trans. Nanobiosci.* 3:237–42

Qu X, Wu D, Mets L, Scherer NF. 2004. Nanometer-localized multiple single-molecule fluorescence microscopy. *Proc. Natl. Acad. Sci. USA* 101:11298–303

Rankin BR, Hell SW. 2009. STED microscopy with a MHz pulsed stimulated-Raman-scattering source. *Opt. Express* 17:15679–84

Rittweger E, Han KY, Irvine SE, Eggeling C, Hell SW. 2009. STED microscopy reveals crystal color centres with nanometric resolution. *Nat. Photonics* 3:144–47

Rust MJ, Bates M, Zhuang X. 2006. Sub-diffraction-limit imaging by stochastic optical reconstruction microscopy (STORM). *Nat. Methods* 3:793–95

Saffarian S, Kirchhausen T. 2008. Differential evanescence nanometry: live-cell fluorescence measurements with 10-nm axial resolution on the plasma membrane. *Biophys. J.* 94:2333–42

Sako Y, Minoghchi S, Yanagida T. 2000. Single-molecule imaging of EGFR signaling on the surface of living cells. *Nat. Cell Biol.* 2:168–72

Schermelleh L, Carlton PM, Haase S, Shao L, Winoto L, et al. 2008. Subdiffraction multicolor imaging of the nuclear periphery with 3D structured illumination microscopy. *Science* 320:1332–36

Schmidt R, Wurm CA, Jakobs S, Engelhardt J, Egner A, Hell SW. 2008. Spherical nanosized focal spot unravels the interior of cells. *Nat. Methods* 5:539–44

Schmidt R, Wurm CA, Punge A, Egner A, Jakobs S, Hell SW. 2009. Mitochondrial cristae revealed with focused light. *Nano Lett.* 9:2508–10

Schmoranzer J, Kreitzer G, Simon SM. 2003. Migrating fibroblasts perform polarized, microtubule-dependent exocytosis towards the leading edge. *J. Cell Sci.* 116:4513–19

Schröder J, Benink H, Dyba M, Los GV. 2009. In vivo labeling method using a genetic construct for nanoscale resolution microscopy. *Biophys. J.* 96:L1–3

Schwentker MA, Bock H, Hofmann M, Jakobs S, Bewersdorf J, et al. 2007. Wide-field subdiffraction RESOLFT microscopy using fluorescent protein photoswitching. *Microsc. Res. Tech.* 70:269–80

Sentenac A, Belkebir K, Giovannini H, Chaumet PC. 2009. High-resolution total-internal-reflection fluorescence microscopy using periodically nanostructured glass slides. *J. Opt. Soc. Am. A* 26:2550–57

Sharonov A, Hochstrasser RM. 2006. Wide-field subdiffraction imaging by accumulated binding of diffusing probes. *Proc. Natl. Acad. Sci. USA* 103:18911–16

Shroff H, Galbraith CG, Galbraith JA, Betzig E. 2008. Live-cell photoactivated localization microscopy of nanoscale adhesion dynamics. *Nat. Methods* 5:417–23

Shroff H, Galbraith CG, Galbraith JA, White H, Gillette J, et al. 2007. Dual-color superresolution imaging of genetically expressed probes within individual adhesion complexes. *Proc. Natl. Acad. Sci. USA* 104:20308–13

Shtengel G, Galbraith JA, Galbraith CG, Lippincott-Schwartz J, Gillette JM, et al. 2009. Interferometric fluorescent super-resolution microscopy resolves 3D cellular ultrastructure. *Proc. Natl. Acad. Sci. USA* 106:3125–30

Sieber JJ, Willig KI, Kutzner C, Gerding-Reimers C, Harke B, et al. 2007. Anatomy and dynamics of a supramolecular membrane protein cluster. *Science* 317:1072–76

Simon SM. 2009. Partial internal reflections on total internal reflection fluorescent microscopy. *Trends Cell Biol.* 19:661–68

Annu. Rev. Cell Dev. Biol. 2010.26:285-314. Downloaded from www.annualreviews.org
by Yale University STERLING CHEMISTRY LIBRARY on 10/08/10. For personal use only.

NanoString Exhibit 1018.029

Smith CS, Joseph N, Rieger B, Lidke KA. 2010. Fast, single-molecule localization that achieves theoretically minimum uncertainty. *Nat. Methods* 7(5):373–75

Stock K, Sailer R, Strauss WS, Lyttek M, Steiner R, Schneckenburger H. 2003. Variable-angle total internal reflection fluorescence microscopy (VA-TIRFM): realization and application of a compact illumination device. *J. Microsc.* 211:19–29

Strack RL, Hein B, Bhattacharyya D, Hell SW, Keenan RJ, Glick BS. 2009. A rapidly maturing far-red derivative of DsRed-Express2 for whole-cell labeling. *Biochemistry* 48:8279–81

Subach FV, Patterson GH, Manley S, Gillette JM, Lippincott-Schwartz J, Verkhusha VV. 2009. Photoactivatable mCherry for high-resolution two-color fluorescence microscopy. *Nat. Methods* 6:153–59

Sun Y, Schroeder HW III, Beausang JF, Homma K, Ikebe M, Goldman YE. 2007. Myosin VI walks "wiggly" on actin with large and variable tilting. *Mol. Cell* 28:954–64

Tagawa A, Mezzacasa A, Hayer A, Longatti A, Pelkmans L, Helenius A. 2005. Assembly and trafficking of caveolar domains in the cell: caveolae as stable, cargo-triggered, vesicular transporters. *J. Cell Biol.* 170:769–79

Taraska JW, Almers W. 2004. Bilayers merge even when exocytosis is transient. *Proc. Natl. Acad. Sci. USA* 101:8780–85

Taraska JW, Perrais D, Ohara-Imaizumi M, Nagamatsu S, Almers W. 2003. Secretory granules are recaptured largely intact after stimulated exocytosis in cultured endocrine cells. *Proc. Natl. Acad. Sci. USA* 100:2070–75

Thompson MA, Lew MD, Badieirostami M, Moerner WE. 2010. Localizing and tracking single nanoscale emitters in three dimensions with high spatiotemporal resolution using a double-helix point spread function. *Nano Lett.* 10:211–18

Tokunaga M, Imamoto N, Sakata-Sogawa K. 2008. Highly inclined thin illumination enables clear single-molecule imaging in cells. *Nat. Methods* 5:159–61

Toomre D, Axelrod D. 2005. Total internal reflection fluorescent microscopy (TIRFM). In *Cell Biology: A Laboratory Handbook*, ed. JE Celis, 3:19–28. Burlington, MA: Elsevier Academic Press. 3rd ed.

Toomre D, Manstein DJ. 2001. Lighting up the cell surface with evanescent wave microscopy. *Trends Cell Biol.* 11:298–303

Toomre D, Steyer JA, Keller P, Almers W, Simons K. 2000. Fusion of constitutive membrane traffic with the cell surface observed by evanescent wave microscopy. *J. Cell Biol.* 149:33–40

Toprak E, Enderlein J, Syed S, McKinney SA, Petschek RG, et al. 2006. Defocused orientation and position imaging (DOPI) of myosin V. *Proc. Natl. Acad. Sci. USA* 103:6495–99

Tsuboi T, McMahon HT, Rutter GA. 2004. Mechanisms of dense core vesicle recapture following "kiss and run" ("cavicapture") exocytosis in insulin-secreting cells. *J. Biol. Chem.* 279:47115–24

Vale RD, Spudich JA, Griffis ER. 2009. Dynamics of myosin, microtubules, and Kinesin-6 at the cortex during cytokinesis in *Drosophila* S2 cells. *J. Cell Biol.* 186:727–38

van de Linde S, Sauer M, Heilemann M. 2008. Subdiffraction-resolution fluorescence imaging of proteins in the mitochondrial inner membrane with photoswitchable fluorophores. *J. Struct. Biol.* 164:250–54

van 't Hoff M, de Sars V, Oheim M. 2008. A programmable light engine for quantitative single molecule TIRF and HILO imaging. *Opt. Express* 16:18495–504

von Middendorff C, Egner A, Geisler C, Hell SW, Schönle A. 2008. Isotropic 3D nanoscopy based on single emitter switching. *Opt. Express* 16:20774–88

Wang CJ, Carlton PM, Golubovskaya IN, Cande WZ. 2009. Interlock formation and coiling of meiotic chromosome axes during synapsis. *Genetics* 183:905–15

Weiger MC, Wang CC, Krajcovic M, Melvin AT, Rhoden JJ, Haugh JM. 2009. Spontaneous phosphoinositide 3-kinase signaling dynamics drive spreading and random migration of fibroblasts. *J. Cell Sci.* 122:313–23

Wennmalm S, Simon SM. 2007. Studying individual events in biology. *Annu. Rev. Biochem.* 76:419–46

Westphal V, Rizzoli SO, Lauterbach MA, Kamin D, Jahn R, Hell SW. 2008. Video-rate far-field optical nanoscopy dissects synaptic vesicle movement. *Science* 320:246–49

Wildanger D, Buckers J, Westphal V, Hell SW, Kastrup L. 2009. A STED microscope aligned by design. *Opt. Express* 17:16100–10

Yazawa M, Sadaghiani AM, Hsueh B, Dolmetsch RE. 2009. Induction of protein-protein interactions in live cells using light. *Nat. Biotechnol.* 27:941–45

Annu. Rev. Cell Dev. Biol. 2010.26:285-314. Downloaded from www.annualreviews.org
by Yale University STERLING CHEMISTRY LIBRARY on 10/08/10. For personal use only.

NanoString Exhibit 1018.030

Yildiz A, Forkey JN, McKinney SA, Ha T, Goldman YE, Selvin PR. 2003. Myosin V walks hand-over-hand: single fluorophore imaging with 1.5-nm localization. *Science* 300:2061–65

Yumura S, Ueda M, Sako Y, Kitanishi-Yumura T, Yanagida T. 2008. Multiple mechanisms for accumulation of myosin II filaments at the equator during cytokinesis. *Traffic* 9:2089–99

Zenisek D, Steyer JA, Almers W. 2000. Transport, capture and exocytosis of single synaptic vesicles at active zones. *Nature* 406:849–54

Zhou M, Wang YL. 2008. Distinct pathways for the early recruitment of myosin II and actin to the cytokinetic furrow. *Mol. Biol. Cell* 19:318–26

Zoncu R, Perera RM, Balkin DM, Pirruccello M, Toomre D, De Camilli P. 2009. A phosphoinositide switch controls the maturation and signaling properties of APPL endosomes. *Cell* 136:1110–21

RELATED RESOURCES:

Olympus Microscopy Resource Center, which has many excellent TIRFM applets: **http://www.olympusmicro.com/primer/techniques/fluorescence/tirf/tirfhome.html**

Zeiss Reference Library, which has good links to reviews on super-resolution microscopy, structured illumination microscopy, and TIRFM: **http://zeiss-campus.magnet.fsu.edu/referencelibrary/index.html**

Nikon MicroscopyU Resource, which has good links and tutorials: **http://www.microscopyu.com/**

A list of fluorophores usable in STED microscopy with optimized parameters and references: **http://www.mpibpc.mpg.de/groups/hell/STED_Dyes.html**

A compendium of historical milestones in light microscopy: **http://www.nature.com/milestones/milelight/timeline.html**

Annu. Rev. Cell Dev. Biol. 2010.26:285-314. Downloaded from www.annualreviews.org
by Yale University STERLING CHEMISTRY LIBRARY on 10/08/10. For personal use only.

NanoString Exhibit 1018.031

Contents

Annual Review of Cell and Developmental Biology

Volume 26, 2010

Enzymes, Embryos, and Ancestors
John Gerhart 1

Control of Mitotic Spindle Length
Gohta Goshima and Jonathan M. Scholey 21

Trafficking to the Ciliary Membrane: How to Get Across the Periciliary Diffusion Barrier?
Maxence V. Nachury, E. Scott Seeley, and Hua Jin 59

Transmembrane Signaling Proteoglycans
John R. Couchman 89

Membrane Fusion: Five Lipids, Four SNAREs, Three Chaperones, Two Nucleotides, and a Rab, All Dancing in a Ring on Yeast Vacuoles
William Wickner 115

Tethering Factors as Organizers of Intracellular Vesicular Traffic
I-Mei Yu and Frederick M. Hughson 137

The Diverse Functions of Oxysterol-Binding Proteins
Sumana Raychaudhuri and William A. Prinz 157

Ubiquitination in Postsynaptic Function and Plasticity
Angela M. Mabb and Michael D. Ehlers 179

α-Synuclein: Membrane Interactions and Toxicity in Parkinson's Disease
Pavan K. Auluck, Gabriela Caraveo, and Susan Lindquist 211

Novel Research Horizons for Presenilins and γ-Secretases in Cell Biology and Disease
Bart De Strooper and Wim Annaert 235

Modulation of Host Cell Function by *Legionella pneumophila* Type IV Effectors
Andree Hubber and Craig R. Roy 261

A New Wave of Cellular Imaging
Derek Toomre and Joerg Bewersdorf 285

Mechanical Integration of Actin and Adhesion Dynamics in Cell Migration
Margaret L. Gardel, Ian C. Schneider, Yvonne Aratyn-Schaus, and Clare M. Waterman 315

Annu. Rev. Cell Dev. Biol. 2010.26:285-314. Downloaded from www.annualreviews.org
by Yale University STERLING CHEMISTRY LIBRARY on 10/08/10. For personal use only.

NanoString Exhibit 1018.032

Cell Motility and Mechanics in Three-Dimensional Collagen Matrices
Frederick Grinnell and W. Matthew Petroll 335

Rolling Cell Adhesion
Rodger P. McEver and Cheng Zhu 363

Assembly of Fibronectin Extracellular Matrix
Purva Singh, Cara Carraher, and Jean E. Schwarzbauer 397

Interactions Between Nuclei and the Cytoskeleton Are Mediated by SUN-KASH Nuclear-Envelope Bridges
Daniel A. Starr and Heidi N. Fridolfsson 421

Plant Nuclear Hormone Receptors: A Role for Small Molecules in Protein-Protein Interactions
Shelley Lumba, Sean R. Cutler, and Peter McCourt 445

Mammalian *Su*(*var*) Genes in Chromatin Control
Barna D. Fodor, Nicholas Shukeir, Gunter Reuter, and Thomas Jenuwein 471

Chromatin Regulatory Mechanisms in Pluripotency
Julie A. Lessard and Gerald R. Crabtree 503

Presentation Counts: Microenvironmental Regulation of Stem Cells by Biophysical and Material Cues
Albert J. Keung, Sanjay Kumar, and David V. Schaffer 533

Paramutation and Development
Jay B. Hollick 557

Assembling Neural Crest Regulatory Circuits into a Gene Regulatory Network
Paola Betancur, Marianne Bronner-Fraser, and Tatjana Sauka-Spengler 581

Regulatory Mechanisms for Specification and Patterning of Plant Vascular Tissues
Ana Caño-Delgado, Ji-Young Lee, and Taku Demura 605

Common Factors Regulating Patterning of the Nervous and Vascular Systems
Mariana Melani and Brant M. Weinstein 639

Stem Cell Models of Cardiac Development and Disease
Kiran Musunuru, Ibrahim J. Domian, and Kenneth R. Chien 667

Stochastic Mechanisms of Cell Fate Specification that Yield Random or Robust Outcomes
Robert J. Johnston, Jr. and Claude Desplan 689

A Decade of Systems Biology
Han-Yu Chuang, Matan Hofree, and Trey Ideker 721

Annu. Rev. Cell Dev. Biol. 2010.26:285-314. Downloaded from www.annualreviews.org
by Yale University STERLING CHEMISTRY LIBRARY on 10/08/10. For personal use only.

NanoString Exhibit 1018.033